Measurement 257 (2026) 118946



Contents lists available at ScienceDirect

Measurement

journal homepage: www.elsevier.com/locate/measurement





Improvement of InSAR displacements based on GNSS station calibration over corner reflector

Alex Alonso-Díaz [a], Dora Roque [b], José Nuno Lima [b], Juan Luis Rodríguez [a], Mercedes Solla [a,*]

[a] CINTECX, Universidade de Vigo, GeoTECH Research Group, 36310 Vigo, Spain
[b] National Laboratory for Civil Engineering, 1700-066 Lisboa, Portugal

ARTICLE INFO

Keywords:
InSAR
GNSS
Calibration
Corner reflector
PSI
QPS
Levelling

ABSTRACT

This article presents an analysis of the effectiveness of performing a calibration through Global Navigation Satellite System (GNSS) data on different approaches of the Interferometric Synthetic Aperture Radar (InSAR). InSAR has become a key technique for monitoring ground surface, but its results often exhibit systematic biases and deviations from ground truth measurements. This study addresses the need for more reliable displacement data by evaluating a GNSS-based calibration approach across three InSAR processing approaches: i) Persistent Scattering Interferometry (PSI) method using the open-source software StaMPS, ii) PSI method using the commercial SARPROZ software and iii) the Quasi-PS method implemented with SARPROZ. Sentinel-1 A/B data from both ascending and descending orbits, covering the period from October 2017 to January 2019, were used. Displacement errors from the same points were modeled using polynomial regressions and calibrated using reference data from GNSS and levelling, both with submillimeter precision. The effectiveness of the calibration was assessed at two levels: locally (via a corner reflector) and globally (via a GNSS baseline several kilometers long). Results show that 25 out of 27 displacement time series required correction in the mean value, with StaMPS showing the greatest need for calibration. The calibration improved the original results at all scales and acted mainly on the mean difference, with linear calibration being the most robust and consistent option. These findings highlight the importance of incorporating ground truth data to enhance InSAR reliability and support its application in geodetic and structural monitoring.

1. Introduction

Understanding the exact accuracy of a geodetic technique is paramount for reliable scientific analysis and informed decision-making. Accurate measurements serve as the foundation for assessing natural hazards, monitoring environmental changes, and ensuring the integrity of critical infrastructure. In geodetic applications, where small deviations can have significant implications, knowing the precision and reliability of a technique allows researchers to quantify uncertainties and establish confidence levels in their findings. Moreover, accurate data is essential for validating models, verifying hypotheses, and detecting subtle changes in the Earth's surface over time. By comprehensively assessing the accuracy of geodetic techniques, scientists can effectively interpret results, identify potential sources of error, and refine methodologies to improve measurement precision and enhance the overall understanding of dynamic Earth processes.

The integration of multimodal data sources (optical and radar) improves monitoring accuracy [1], accelerates classification, and provides additional information for analysis [2]. Global Navigation Satellite Systems (GNSS), Interferometric Synthetic Aperture Radar (InSAR), Levelling and Corner Reflectors (CR) represent cutting-edge technologies revolutionizing geodetic monitoring [3]. Their integration offers unparalleled insights into surface deformations, aiding in seismic risk assessment, fault modeling, and tectonic studies [4]. This paper explores the synergistic benefits derived from combining these technologies, with a focus on the calibration of original InSAR time-series data using GNSS measurements.

GNSS comprises a network of satellites providing precise positioning data globally. Leveraging signals emitted by satellites, GNSS receivers determine precise locations on Earth's surface, enabling the monitoring of crustal movements with submillimeter-level accuracy over time [3]. InSAR utilizes radar technology mounted on satellites that operates

* Corresponding author.
E-mail address: merchisolla@uvigo.es (M. Solla).

https://doi.org/10.1016/j.measurement.2025.118946
Received 2 August 2024; Received in revised form 1 August 2025; Accepted 4 September 2025
Available online 7 September 2025
0263-2241/© 2025 The Author(s). Published by Elsevier Ltd. This is an open access article under the CC BY license (http://creativecommons.org/licenses/by/4.0/).

independently of weather and environmental conditions to generate continuous monitoring and high-resolution maps of ground displacements [2]. By analyzing the phase differences between radar signals acquired from two passes over the same area, InSAR can detect surface movements. This technique is particularly useful for monitoring large-scale deformations [5]. CRs are passive targets placed on the Earth's surface to ensure radar signal reflections in InSAR applications serving as reference points for the InSAR processing. These artificial targets improve the coherence and reliability of SAR data, facilitating more accurate displacement measurements [6], playing a crucial role in validating and calibrating InSAR observations, especially in areas with sparse natural features.

The integration of GNSS and InSAR data offers several advantages, including improved accuracy, temporal coverage, and spatial resolution of surface deformation measurements [7]. GNSS provides high-precision ground control points that serve as reference data for the validation and calibration of InSAR-derived displacements, thereby increasing the reliability of deformation maps. Calibrating InSAR data with GNSS involves the alignment and validation of SAR-derived displacements against precise GNSS observations—over the Line-Of-Sight (LOS). By comparing InSAR with GNSS displacements, systematic errors in SAR data can be identified and corrected. As a result, the integration and calibration process significantly improve the overall accuracy and robustness of InSAR-based deformation monitoring products [7]. One of the main challenges in integrating GNSS and InSAR data lies in the sparse distribution of coherent scatterers in InSAR results, and the uncertainty associated with spatial misalignment between datasets. To address these issues, the proposed approach leverages the use of CRs and naturally coherent structures, such as buildings.

In this study, a comprehensive calibration of displacements obtained using InSAR technology was conducted. The calibration process involved analyzing six different InSAR configurations (different directions, software and algorithms). The InSAR time series were compared with GNSS observations over real points (buildings and CRs). Errors in the InSAR displacement time series were modeled through polynomial regressions and used to calibrate the observations. The effectiveness of the calibration was evaluated both locally, by comparing vertical displacements with levelling measurements, and globally, using information from a GNSS station. This multi-faceted approach aimed at enhancing the accuracy and reliability of InSAR measurements in deformation monitoring applications.

The novelty of this research lies in the integrated use of InSAR, GNSS, and CRs to implement a calibration methodology applied directly to displacement time series of real points, rather than relying on approaches based on the velocity data and different scatterers selection criteria in the vicinity of GNSS stations that include generalizations, errors and finally reduce the quality of the results. In addition, a comprehensive quantitative statistical framework has been developed to evaluate the contribution of each calibration strategy, to identify which components of the InSAR signal are effectively corrected, and to assess effects like overfitting. The calibration proposed is further validated through both local and global comparisons with independent geodetic measurements, including GNSS and precise levelling, thereby ensuring the reliability and robustness of the proposed approach across different spatial and temporal scales.

This paper is organized as follows: The Materials and Methods section provides a comprehensive overview of the study, including a review of the state of the art in GNSS and InSAR technologies. It details the area of study and the corner reflectors used for data collection. This section also explains the InSAR methodologies and processing techniques, as well as the GNSS and levelling processes involved. Additionally, it covers the calibration and validation procedures proposed and the statistical analysis metrics employed. The Results and Discussion section presents a comparison of displacements obtained from various InSAR configurations, discusses the calibration functions applied, and evaluates the local and global validation results for the calibration proposed. Finally, the Conclusion section summarizes the key findings of the study and further work, reflecting on the implications and potential applications of the improved calibration methods.

2. Materials and methods

2.1. GNSS and InSAR overview

InSAR technology presents the following problems as a stand-alone technique: i) Errors (orbital, atmospheric, topographic and temporal decorrelation noise), ii) Insensibility (north movements estimation and rapid movements), iii) Absolute reference necessity, and iv) Target-nature limitations [8]. Most of these problems can be attached using GNSS data (Table 1), enhancing the capabilities of the technique [9]. Other advantages are the different nature and direct comparison between GNSS and InSAR data [10].

Studies that combine GNSS and InSAR have explored a wide range of SAR products (satellite images) and algorithms (Table 2), demonstrating their applicability across various research fields. These include land subsidence [20,21], earthquake monitoring [8,22], atmospheric effects [12,23,24], surface deformation [18,25,26,27], volcanic activity [28,29], landslide analysis [30,31], and infrastructure monitoring [32,33]. These studies have concluded that using Persistent Scatterers methods (PS) is a better option than using Distributed Scatterers (DS) due to the lower integration error [20]. Additionally, [6] demonstrated that the original InSAR results require calibration of the mean (failed to pass the Student's *t*-test), and lower-resolution images require more correction [34].

Moreover, some projects have analyzed the capacities of combining GNSS with InSAR from various perspectives: i) referencing and decomposition. European Ground Motion Service (EGMS) over the European continent with Sentinel-1 images [27]; ii) calibration and validation with a total of 621 GNSS sites over Italy [18]; iii) involving CRs to create infrastructure — Cyprus Continuously Operating Natural Hazards Monitoring and Prevention System (CyCLOPS) over Cyprus [38] and Hungary with Integration of Sentinel-1 Interferometry and GNSS Networks (ISIGN) [17]; and iv) involving other technologies such as

Table 1
InSAR problems and possible solutions.

InSAR problems	Solutions provided by literature
i) Errors:	
Orbital	−Precise orbit with GNSS in satellite [11] −Remove OPS (Orbital Phase Screens) [12] −Improve baseline detection (GNSS) [13,14]
Atmospheric (Troposphere and Ionosphere)	−GNSS calibration estimates APS (Atmospheric Phase Screen), low-frequency displacement components and atmospheric delay. [10] −Fitted with trend surface or models [15]
Topographic	−Limited with DEMs (Digital Elevation Models) [8]
Temporal decorrelation noise	−GNSS network tie spatial displacement measurements, improving unwrapping estimation [16]
ii) Insensibility to:	
Ground movement in the satellite track direction	To obtain 3D ground displacement maps [8]: − Compensated. Combining InSAR measurements from complementary LOS directions (at least 3) − Combining InSAR with other techniques (GNSS or levelling). − Modeling or numerical simulation.
Rapid movements	−GNSS detects, confirms and correct missing cycles [17]
iii) Absolute reference necessity	− Knowledge of the relative motion − GNSS like reference point and calibration technique [18]
iv) Target-nature limitations	− Machine learning models [19] − GNSS calibration

Table 2
GNSS and InSAR works relative to images and algorithms.

Satellite images		
Band	Satellite	Reference
X	COSMO-SkyMed	[20,21]
	TanDEM	[14]
C	Sentinel	[20,25–28,33,35]
	ENVISAT	[15,18]
L	ALOS/PALSAR	[8]
Algorithm		
Method	Software	Reference
DInSAR	ROI_PAC	[8]
PSI	Gamma	[20,27]
	Stamps	[21,25]
	SARPROZ	[32,33]
SBAS	GMTSAR	[36,37]
Hybrid PS/DS	Gamma	[28]
	SqueeSAR	[34]

Compact Active Transponders (CAT) in Slovenia [30].

The two main applications for GNSS and InSAR combination are validation and calibration. On one hand, the main findings for validation are: i) Comparing uncertainty with Continuous-GNSS. For Sentinel images the deformation rates were consistent [25]; the velocity LOS differences are 2.8 and 2.6 mm/yr for PS and Distributed Scatterers (DS), respectively [35]; and the correlation coefficient R^2 was of 0.72 [39]. Moreover, for Small BAseline Subset method (SBAS) the precision is 1.5 mm/yr with European Remote Sensing Satellite Mission (ERS) images [40], the displacement difference was 6 and 5 mm for ascending and descending orbits with ALOS/PALSAR images [23], and the correlation with time series is high [41]. ii) Comparing with Non-Permanent Sites (NPS) GNSS the velocity difference is less than 5 mm/yr for about 85 % of the 46 stations with a maximum of 10 mm/yr [20].

The main conclusions to validate the velocity accuracy of the GNSS and InSAR are that there exists a good agreement for Sentinel-1 and of about 2 mm/yr for COSMO-SkyMed compared with Continuous-GNSS [20]. Considering the methods, SqueeSAR has a precision of 0.6 mm/yr [21], and DInSAR decreases the Root Mean Squared Error (RMSE) from 9.3 to 5.8 cm [8]. Finally, about the component's correlation, Pearson Coefficient is 0.19 [18] and 0.34 [42] for vertical component and 0.028 for horizontal components [18].

On the other hand, the calibration methodology is based on the velocity data and the difference consists of the scatterers selection criteria: i) the closest to the GNSS station [21,35], ii) the mean within an influence area [20,26], iii) the one with the strongest decorrelation [18], iv) the one with the least squared phase variation [43], v) the weighted distance average in an area [15], and vi) the weighted average by coherence [21]. Furthermore, another topic is the method used to calibrate the rest of the points (over an interpolated model [18], over a velocity component associated with an error [21], and over proximity [20]).

2.2. Area of study and corner reflectors

The study area is at the National Laboratory for Civil Engineering (LNEC) in Lisbon, Portugal (38.7594 N, 9.1399 W). The complex is in the northern part of Lisbon near the Lisbon International Airport Humberto Delgado in the Alvalade district on Brazil Avenue (Fig. 1), the LNEC campus was inaugurated in 1952 and comprises several buildings dedicated to multiple departments [44]. The area features significant vegetation.

The Gulbenkian building (bottom right in Fig. 1a) includes a continuous GNSS antenna on the roof and in the garden in front is a double CR (dCR), which provides stable reference points for both

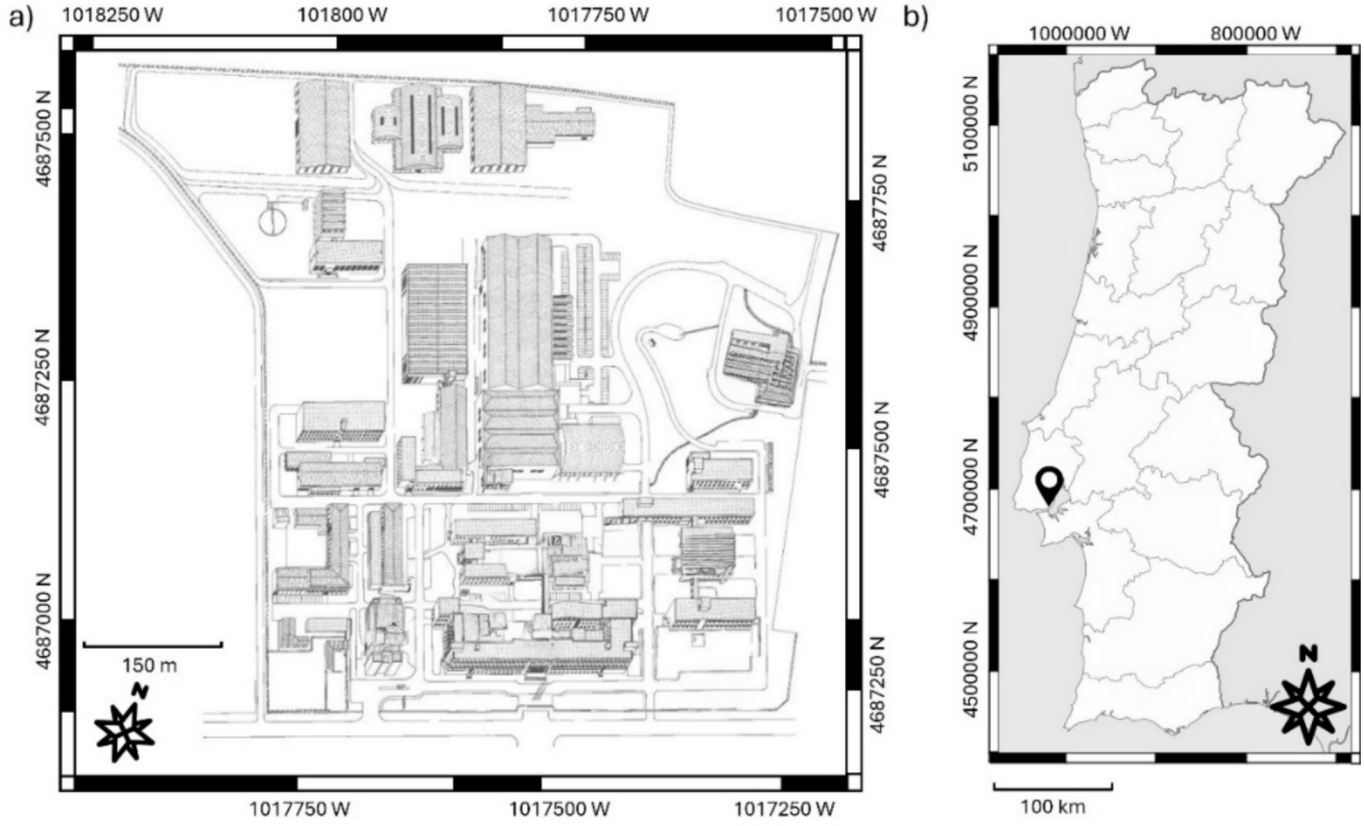


Fig. 1. (a) Map of LNEC complex [45]; (b) Lisboa location in mainland Portugal map. Coordinates Reference System (Datum 73/UTM zone 29 N — EPSG:27429).

ascending and descending orbits of the Sentinel-1 constellation data and is also monitored by GNSS. For a better understanding, Fig. 2 presents a view of these elements.

Corner reflectors are artificial targets used in remote sensing, particularly in InSAR applications, that provide scatterers with high coherence and low phase noise [17]. CRs corrects topographically the InSAR results and permits the acquisition of the time series of specific points, analyzing the displacement time series of specific scatterers without averaging, which would diminish the technique's performance. The dCR installed in LNEC complex consists of a concrete foundation with an aluminum structure of perforated sheets, designed for both geometries [7] (Fig. 2c). The dCR is formed by two rectangular trihedrals united by their vertical edges. Each trihedral is directed towards the LOS of a Sentinel-1 geometry: ascending pass relative orbit 45 and descending pass relative orbit 125. Both trihedrals are oriented horizontally towards each LOS, but not vertically. The vertical edge resulting from the union of both trihedrals is topped by a GNSS antenna in continuous operation. A choke-ring model is used to minimize multipath. Besides the dCR, there is also an individual CR following a triangular trihedral model in LNEC. The triangular trihedral CR (TTCR) is monitored in the vertical direction with levelling technology. It is located 400 m away from the dCR and was used for validating locally the calibration proposed between (Gulbenkian building and dCR).

In this study, the dCR and the building roof serve as ground control points for comparing InSAR and GNSS results, as these elements provide coherent scatterers for InSAR measurements and are monitored by GNSS for direct comparison. The location and proximity between both points mitigate effects like geodynamics or atmospheric [17], maximizing an accurate datum connection [38].

2.3. InSAR

Technology that offers immediate, cost-effective, and extensive surface monitoring, providing essential information for effective management [46]. This is achieved through an active remote sensing technology Synthetic Aperture Radar (SAR) that works with microwave signals. SAR sensors obtain highly stable imaging systems, mostly over airborne and spaceborne platforms. Microwave properties such as amplitude, phase, and polarization from SAR images inform about surface characteristics [46].

InSAR creates interferograms (IFGs) through the radar phase data from SAR products. This enables continuous monitoring of surface changes over time, producing deformation maps, displacement time series, and additional information such as height and coherence over large areas [47]. Nonetheless, due to InSAR problems and uncertainties, in some applications, it is still not considered a stand-alone technique [47].

As presented in Table 1, one of the InSAR problems is the target-nature limitation associated with the method, because each of them has pros and cons. They can be grouped by the target analyzed (Table 3) into: i) Point target, associated with the dominant signal of a single element from a resolution cell to track deformation providing high quality for the few selected points, and ii) Distributed target, where many scatterers from the cell contribute to studying the deformation. The most popular techniques for both groups are Persistent Scatterer Interferometry (PSI) and SBAS, respectively. Theoretically, the first group obtains more accurate results but is affected by vegetation reducing the coherence and limiting the scatterers' density. For that reason, there exists an intermediate group of techniques PS/DS that are the hybrid approaches, which with coherence restrictions involve the IFGs of the other methods. Quasi-PS (QPS) and SqueeSAR are techniques of that group.

2.3.1. Methods

Since the CRs are oriented for Sentinel-1 A/B satellite constellation, it would not be possible to use another type of initial data. Working with complementary images to be able to convert the LOS information to vertical and horizontal components. Regarding the methods, a total of 6 tests (Table 4) were developed using different algorithms (techniques and software). The purpose of all these tests is to draw conclusions about the precision and characteristics of each configuration since the area of study does not fit exactly for any InSAR method (urban area with vegetation) and each software has differences that determine the result (open source against commercial and better accuracy demonstrated [6]).

About the methods: i) QPS is an advanced technique to estimate ground average deformation, which expands PSI to include partially coherent targets [48]. It considers a multi-master graph and it uses coherence as weight for the filtered interferometric phase [49]. Therefore, parameter estimation is performed based on a subset of low-noise IFGs, dependent on each scatterer, enabling the detection of targets that were not coherent for all dates. ii) PSI is a full-processing chain for ground average deformation trend that uses a star graph (single master configuration with one master and the rest are slaves) [5]. In Fig. 3 are presented the network connections for the different methods and orbits.

2.4. GNSS & levelling

GNSS comprises constellations of satellites such as Galileo, NAVSTAR, GLONASS, and BeiDou to provide a navigation system able to



Fig. 2. (a) GNSS antenna installed on the roof; (b) 3D view of the Gulbenkian building and the garden in front highlighting the GNSS and dCR locations; and (c) dCR view.

Table 3
Information about the different InSAR methods.

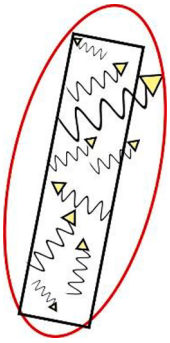
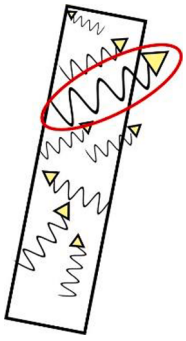
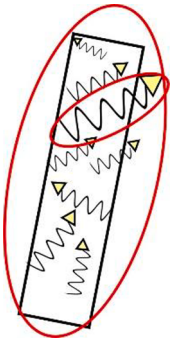
Approach	Distributed Targets	Point-Like Scatterers	Hybrid
Representation of the Sentinel-1 SAR pixel (azimuth and range), including the track angle (descending direction) and reflection points across the pixel. The ellipse in red highlights the specific reflection area used by each approach.			
Most used techniques	SBAS	PSI	QPS and SqueeSAR

Table 4
Information about the different InSAR configurations.

Flight direction	ASC		DSC	
Track	45		125	
Mode	Interferometric Wide (IW)		IW	
Subswath	2		1	
Polarization	VV			
Data acquisition	18:34 h		6:43 h	
Incidence angle	40.61°		35.63°	
Timeline	10/10/2017–28/12/2018		16/10/2017–28/12/2018	
Method	PSI	QPS	PSI	QPS
Software	SNAP & StaMPS	SARPROZ	SNAP & StaMPS	SARPROZ
Master image	01/06/2018	–	26/05/2018	–
Connections	74	731	73	771

provide position, velocity and time over the Earth's surface. That technology contributes to obtaining highly accurate and punctual 3D surface measurements at a point materialized with an antenna connected to a receiver [50]. The precision depends on many variables (equipment, location, and weather conditions) and, under certain conditions, it can obtain sub-millimetric accuracy with better results in the horizontal direction rather than in the vertical [26]. However, the main limitation of this technique is the spatial sampling density of GNSS stations [10].

In this study, two GNSS baselines were considered:

- The first baseline was formed by two antennas at LNEC: the reference antenna was installed on a metallic rod on the roof of Gulbenkian building (Fig. 2a), and the second antenna was mounted on the dCR (Fig. 2c) with a baseline of 38 m. The equipment involved Topcon GB-1000 receivers and choke-ring antennas. With a 30-second measurement cadence in static mode, the software used to calculate the daily relative displacements of the dCR antenna concerning the Gulbenkian antenna was Topcon Pinnacle. As the baseline was small, a simplified model was used, considering L1 and the Goad-Goodman atmospheric model [51]. Over the GNSS information between dCR and Gulbenkian building, it was necessary to do two different corrections: i) a translation, because the dCR and the GNSS antenna suffered a slight inclination during a temporal (it was seen on the time series with a punctual jump); and ii) a detection and removal of the component caused by the inclination that the CR concrete base experienced during its stabilization phase. For this, levelling measurements on the corners of the base were used to determine the position of the GNSS antenna.
- The second GNSS baseline used in the study had a length of 4 km and was formed by the Gulbenkian building antenna at LNEC and the permanent station IGP0 from the ReNEP network (a national network of continuous GNSS stations in Portugal, https://renep.dgterritorio.gov.pt/node/77) located on the roof of the building Direção-Geral do Território (DGT). For a long baseline like Gulbenkian – IGP0, the algorithm provided by Pinnacle was not appropriate, due to the limitations associated with modelling tropospheric delay in vertical direction; therefore, the CSRS-PPP software by the Canadian Space Reference System [52] was used instead to compute the daily coordinates of both antennas through the Precise Point Positioning method. Relative displacements between the IGP0 antenna and the Gulbenkian building were determined from the coordinate differences.

To achieve a more comprehensive analysis, it was converted the GNSS data to LOS using equation (1) from [53]. Where dUp, dN and dE are the GNSS displacements; θ is the SAR incidence angle; α is the SAR satellite orbit inclination; αh is the SAR satellite heading and φ is the latitude.

$$\left.\begin{aligned} dLOS &= dUp^{*}cos\theta - sin\theta[dN^{*}\cos\left(\alpha h - \frac{3\pi}{2}\right) + dE^{*}\sin\left(\alpha h - \frac{3\pi}{2}\right)] \\ \alpha h^{ASC} &= \arcsin\left(\frac{cos\alpha}{cos\varphi}\right) \\ \alpha h^{DSC} &= \pi - \arcsin\left(\frac{cos\alpha}{cos\varphi}\right) \end{aligned}\right\} \quad (1)$$

It was calculated the propagation errors in relative displacements (Table 5) confirming the submillimeter precision for GNSS data between Gulbenkian building and dCR, and levelling. Moreover, the standard deviations for each case were obtained (Fig. 4).

In-situ measurements from levelling were also collected for two monitoring networks on LNEC campus. The first network consisted of the dCR reflective centers, the corners of the concrete base where the dCR is installed and two nearby points, one of them considered stable. The data from this network was used to correct the GNSS antenna position due to the tilt of the dCR concrete base. The second monitoring network was formed by the TTCR, the corners of the concrete base where it is installed and a nearby point considered stable. The data from this network was used to local level validation of the calibration proposed. Observations have an error of 0.10 mm (Table 5).

2.5. Calibration and validation proposed

The InSAR results contain the components of equation (2), where the deformation component is the information of interest, and the rest are nuisances that we seek to minimize. In equation 2, it is indicated the dependency on other factors for the nuisance components. Therefore, estimating these components theoretically is extremely complex [35].

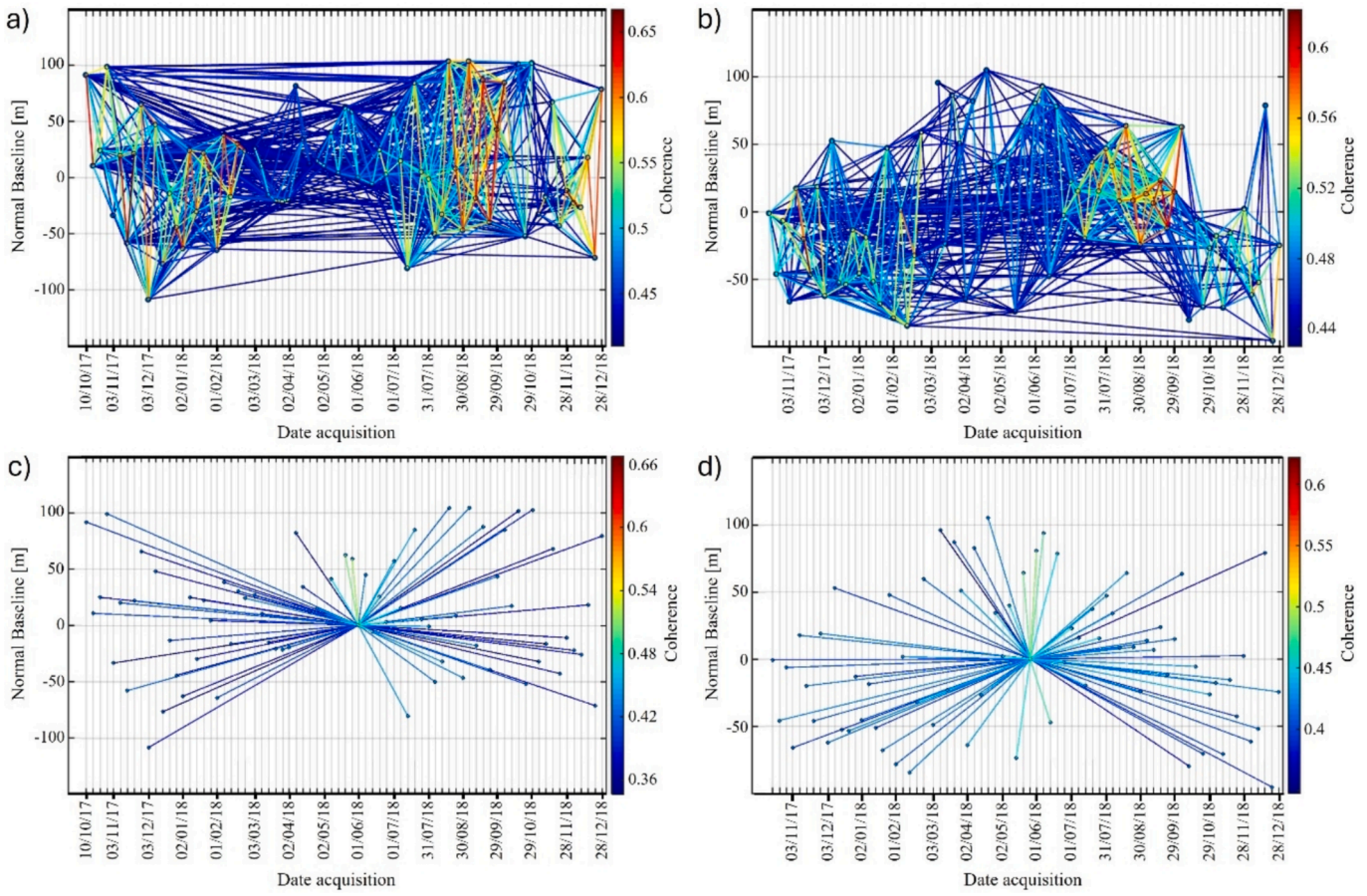


Fig. 3. Images graph for each method and orbit (a) QPS for ASC; (b) QPS for DSC; (c) PSI for ASC; and (d) PSI for DSC.

Table 5
Average relative error in mm.

	Ascending	Descending	Vertical	Horizontal
LNEC (dCR-building)	0.72	0.76	0.90	0.32
Levelling (TTCR-TTCR)	–	–	0.10	–
IGP0 (building-building)	2.95	3.22	3.23	2.30

That is the reason why it is common to perform a calibration using another technology with higher resolution (under certain conditions).

$$\Phi_{InSAR} = \Phi_{deformation} + \Phi_{topographic} + \Phi_{atmospheric} + \Phi_{orbital} + \Phi_{noise}$$
$$\left.\begin{aligned} \Phi_{topographic} &= F(Baseline, Lookangle, Area) \\ \Phi_{atmospheric} &= F[\Delta time, phasedelay(troposphere, Ionosphere)] \\ \Phi_{orbital} &= F(baselineandorbitdetection) \end{aligned}\right\}$$
$$\Phi_{noise} = F(seasonalcomponent, decorrelation, space, Area)$$

To strengthen the calibration process, it is important to address potential temporal and spatial misalignments between the GNSS data and the InSAR measurements:

- Temporal alignment: GNSS data were processed daily, ensuring that for each InSAR acquisition date, a corresponding GNSS observation is available. While GNSS data represent daily averages and InSAR captures instantaneous measurements, any discrepancies due to atmospheric contributions are minimal for the short baselines considered (40 m, 400 m, and 4 km). This is because atmospheric variability over such distances is negligible and largely cancels out in relative displacement calculations. Additionally, both GNSS and InSAR datasets underwent atmospheric correction procedures to further mitigate residual atmospheric effects. Referring to thermal dilation effect, it was considered as noise because the technology levelling (accuracy 0.1 mm) detected only a seasonal movement with an amplitude of ~ 0.5 mm compatible with the effect of soil moisture variations, not temperature. GNSS data were averaged daily to maximize accuracy and obtain more precise ground-truth results.
- Spatial misalignment: although there is a fixed offset between the GNSS antenna phase center and the CR, they are rigidly attached to the same metal structure, eliminating the possibility of relative movement over time. Since the analysis focuses on time-series of coordinate changes relative to a common reference epoch, the static offset does not affect the results. However, absolute positioning differences due to possible settlement of the structure must be considered, with that aim the entire LNEC system (comprising two CRs and the GNSS antenna) is mounted on a concrete parallelepiped resting on a grass surface, whose stability is monitored via four levelling marks placed on its upper corners.

To provide a clear and structured understanding of the methodology, the following workflow diagrams (Fig. 5) outline the sequential processes undertaken for the implementation of the calibration procedure, as well as for the subsequent local and global validation stages. These diagrams serve to illustrate the methodological framework adopted in this study and to facilitate the reproducibility of the approach.

Once the comparison between the InSAR-GNSS displacement time series is established, for the points on the dCR and the Gulbenkian roof, the offset between both time series is determined over time and the error graph is obtained. Different polynomial regressions are evaluated on this error graph based on the coefficient of determination (R^2), from linear to third-degree, managing between underfitting and overfitting –

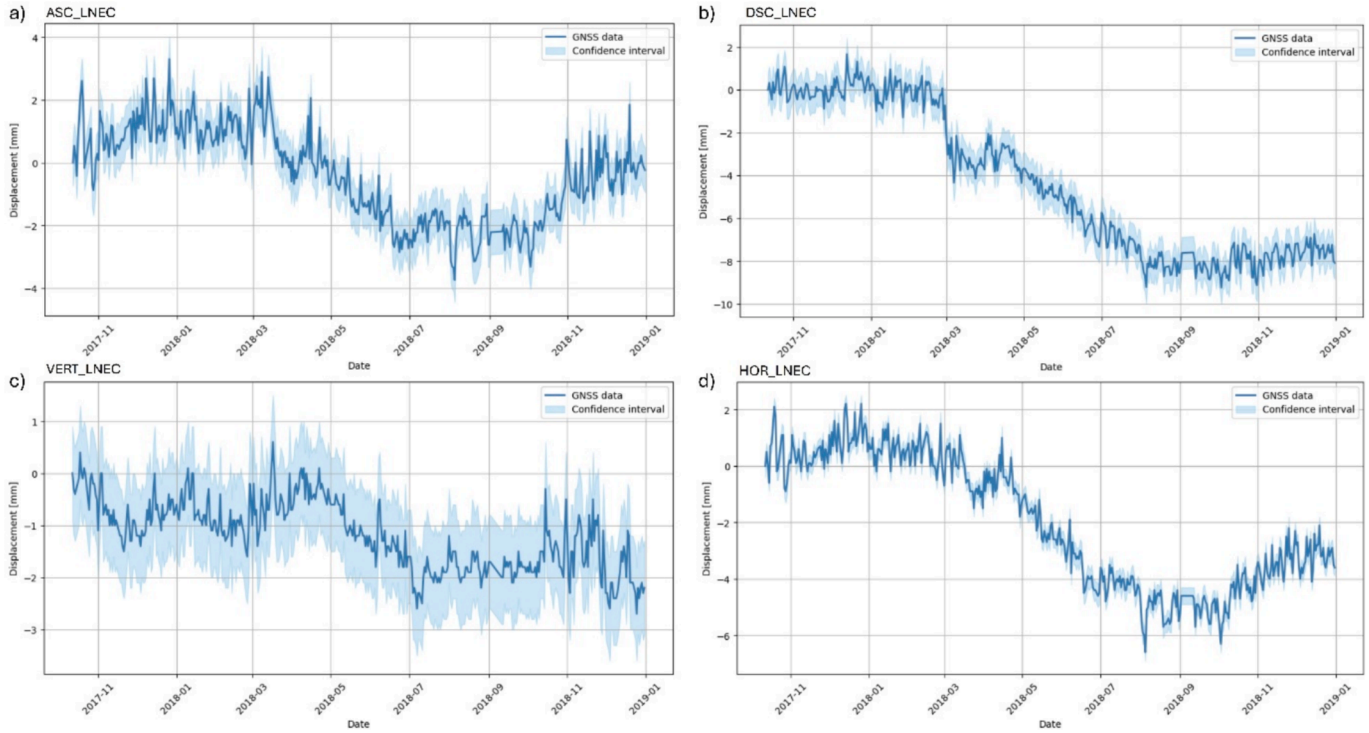


Fig. 4. GNSS displacement time-series between dCR and Gulbenkian building with standard deviation. (a) Ascending LOS; (b) Descending LOS; (c) Vertical component; and (d) Horizontal component.

calibration functions.

The calibration of the InSAR displacements is performed by adding each calibration function to the InSAR displacement time series of the scatterers. The proximity of the dCR to the building theoretically enables to propose a general and common correction for distant areas. Additionally, performing the calibration between anchored elements eliminates the possibility of correcting seasonal components such as groundwater level, gradients, and others, which are not common to other points.

The validation process is divided into a local and a global level (Fig. 6), comparing with two different techniques like GNSS and levelling. While GNSS validation is performed for LOS, vertical, and horizontal components; validation with levelling is limited to the vertical component. Fig. 6 presents the points of interest; where A is the location of the dCR monitored by GNSS, B is the GNSS antenna on the Gulbenkian building, C is the TTCR installed in LNEC monitored by levelling, and D is the GNSS station IGP0 (38.7260 N, 9.1585 W). The local level validation is between points with ~ 400 m distance, and the global validation level is about ~ 4 km distance.

2.6. Statistical analysis

In literature the most used metric to compare InSAR and GNSS results is the velocity difference, and in [23] the three skill scores are mentioned: Compound Relative Error (CRE), Mean Absolute Error (MAE) and Root Mean Square Error (RMSE). Informing only about errors: relative, average magnitude and average magnitude penalizing large deviations, respectively. In the present research, a complete statistical analysis that informs about tendencies, averages and errors is proposed. For that, Pearson correlation coefficient is used for the tendency, Welch's *t*-test for the median and [MAE, Euclidean Distance (ED), and standard deviation (SD)] for the error analysis.

About the error analysis, all the metrics mentioned enhance the understanding. MAE measures the average of the absolute errors; ED informs about the dissimilarity between two time series for common epochs in all dimensions; and SD is used to study the error dispersion. Pearson and Welch's *t*-test metrics involve an initial statistical hypothesis that is either accepted or rejected based on its p-value, the rest of the metrics present relative values.

3. Results and discussion

3.1. Comparison of displacements from different InSAR techniques

After obtaining the relative displacement time series between points A and B in Fig. 6 (dCR monitored by GNSS and Gulbenkian building with a GNSS station, respectively) for each configuration (Table 3), the different configurations involve the algorithm (software and method) and direction (ascending and descending LOS, vertical, and horizontal). In Fig. 7, the time series are visually compared. These results appear comparable both among themselves and with our validation technique (GNSS data with 12-day moving average for clarity), thus seeming representative of our target points A and B. It is noteworthy that in the case of the StaMPS software, standard processing did not yield scatters A and B and needed a less restrictive processing that affected the noise mitigation.

The DSC direction results contribute to the main part of the time series, as both the vertical and horizontal displacement time series have a similar form to the DSC, which appears to yield less similar time series than the ASC. From Table A1 in Appendix A and Fig. 7, it can be stated that regarding the software (StaMPS results have higher variability than those obtained by SARPROZ). According to methods, QPS shows less deviation and fits better than PSI to the GNSS data, except in the ascending direction. Ordering the results on the level of adjustment with the GNSS for PSI method are (ASC, DSC, horizontal, and vertical); whereas for QPS, the order is DSC, horizontal, vertical, and ASC.

3.2. Calibration functions

After representing the time series of the errors for the common dates

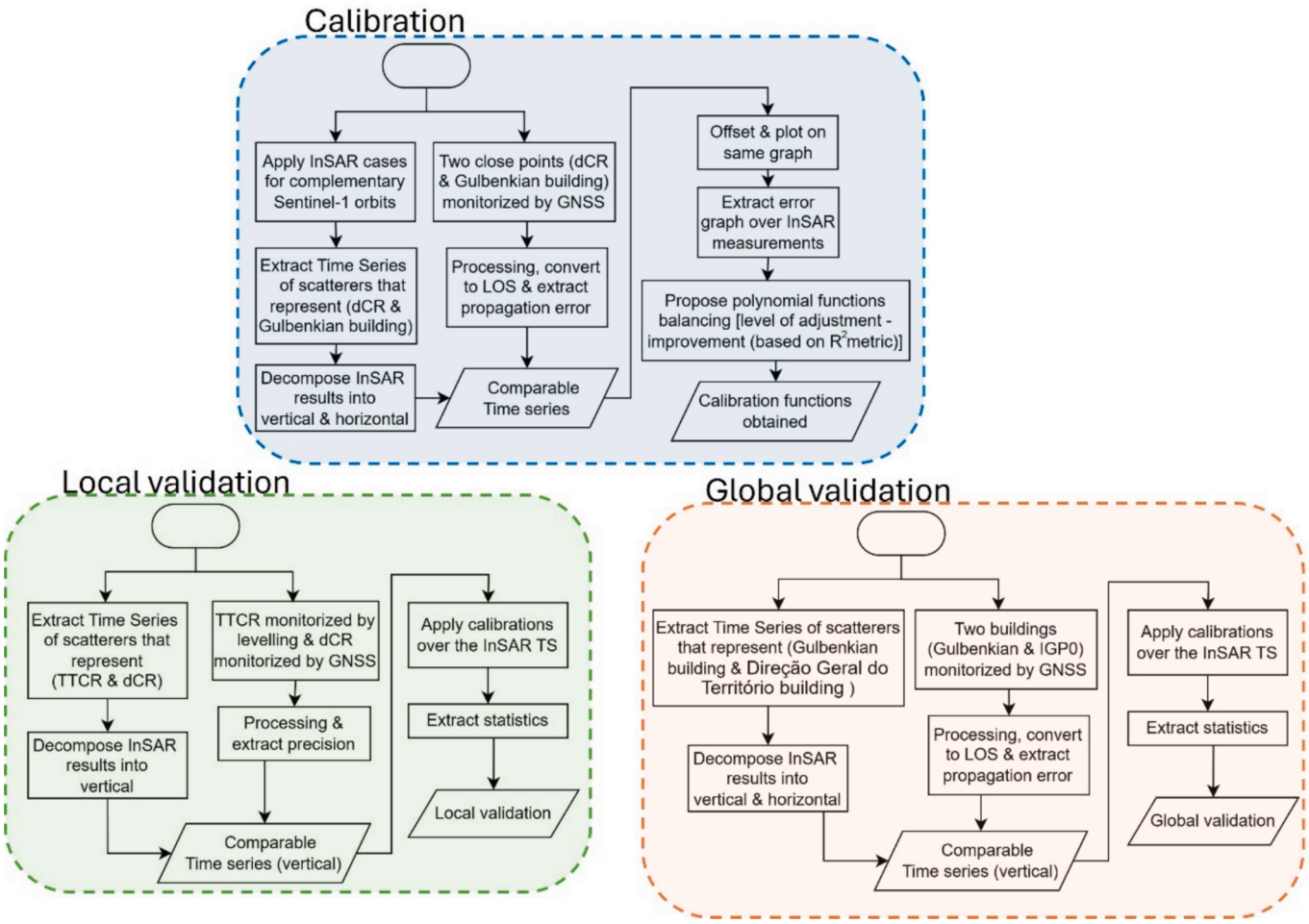


Fig. 5. Flowcharts describing the sequential steps for InSAR calibration and its validation at local and global scales.



Fig. 6. Map of Lisbon city highlighting the points of interest for the local and global level validation. (a) dCR monitored with GNSS, (b) GNSS antenna on the Gulbenkian building, (c) TTCR monitored with levelling, and (d) IGP0 GNSS station. Coordinates Reference System (Datum 73/UTM zone 29 N — EPSG:27429).

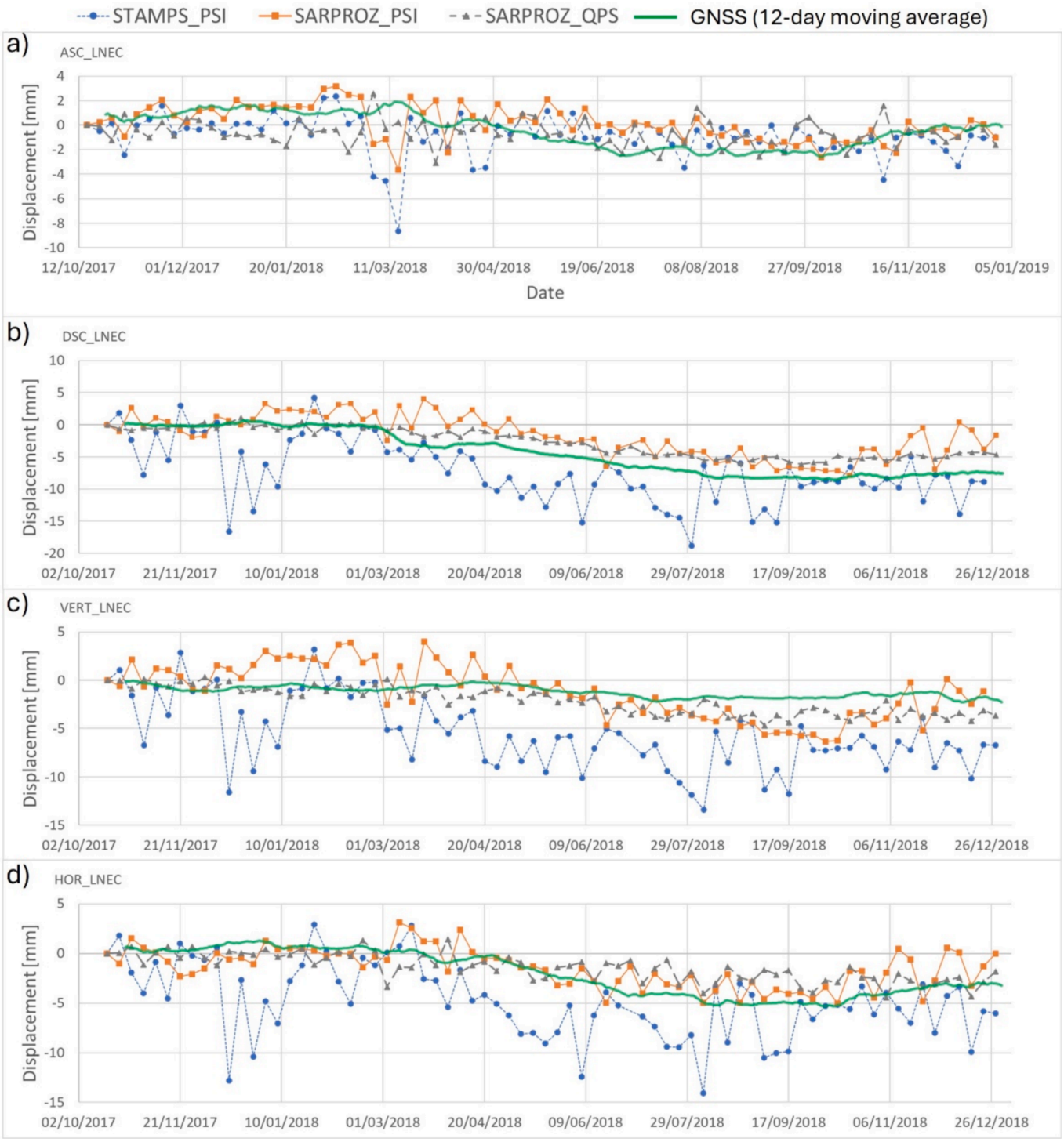


Fig. 7. InSAR and GNSS displacement time series for the relative displacement between dCR and Gulbenkian building in LNEC for (a) Ascending; (b) Descending; (c) Vertical; and (d) Horizontal direction.

(74 points) between InSAR and GNSS between points A and B in Fig. 6, the time series was fitted to polynomial functions, which will serve as our calibration for the rest of the scatterers. These options were chosen based on the R^2, considering the complexity of the equation with the correlation index, and balancing between over and underfitting. Table 6 summarizes the different calibrations proposed. In Fig. A1 from in Appendix A, all the adjustments proposed for the different configurations with the equation and the R^2 are presented.

The following Figs. 8–11 represent the results for the ascending, descending, vertical and horizontal directions. They present the evolution of the different metrics (Pearson correlation, MAE, ED, and SD) for each case with the different adjustments proposed. If the bar's contour is red, it means that the hypothesis (both time series have significant correlation) is not accepted due to the p-value significance. Moreover, if the bar's contour is a black dashed line, it means the calibration did not improve the original results. Relative to the different metrics, an improvement is indicated by an increase in the Pearson metric, and by a reduction in the rest of them. These results, along with their evolution, are important for justifying which calibration of the proposed methods is the most appropriate, as well as for assessing

Table 6
Number and type of adjustment proposed for the different configurations.

	PSI		QPS
	StaMPS	SARPROZ	SARPROZ
Ascending	2 (Linear and third-degree polynomial)	3 (Linear, and second and third-degree polynomial)	2 (Linear and third-degree polynomial)
Descending	2 (Linear and second-degree polynomial)	2 (Linear and third-degree polynomial)	2 (Linear and third-degree polynomial)
Vertical	2 (Linear and second-degree polynomial)	2 (Linear and third-degree polynomial)	2 (Linear and third-degree polynomial)
Horizontal	2 (Linear and second-degree polynomial)	2 (Linear and third-degree polynomial)	3 (Linear, and second and third-degree polynomial)

potential signs of overfitting when comparing them with both local and global validations results.

The evolution of each metric concerning the complexity of the calibration model can present the following scenarios: deterioration, insignificant improvement, non-uniform scaled improvement, or uniformly scaled improvement. As expected, most of the metrics improve, but the most interesting aspect is understanding the behavior and nature of some of these metrics. For example, about the Pearson correlation, that metric shows a significant deterioration in the case of PSI with StaMPS when the improvement is evident when visualizing the time series. This is because this coefficient cannot correctly handle time series that fluctuate one over the other.

Regarding the MAE, ED, and SD metrics, the combined evolution informs about what the calibration has acted upon. If all three metrics improve in a uniformly scaled manner, it means that the calibration has reduced both the large errors and the general dispersion of the errors, as seen in the case of SARPROZ_QPS in the vertical direction. Another scenario can be observed in the case of StaMPS_PSI in the horizontal direction, where MAE and ED improve more than SD. This indicates that the calibration has primarily targeted large errors rather than the general dispersion. In the case of SARPROZ_QPS in the vertical direction, MAE and SD shows similar improvement while ED shows less improvement. This means that the errors are being reduced uniformly without significantly affecting the large errors.

Therefore, in general, the calibration mainly addresses the absolute average of the errors, MAE. However, for example, in the case of StaMPS_PSI in the ascending direction, ED and SD improve more than MAE, which means that the calibration has reduced the overall variability of the errors and the magnitude of the large errors without reducing the absolute average as much.

Table 7 shows the mean difference for the different cases comparing the whole amount of data from GNSS (about 430 epochs) and InSAR displacements over the same periods. The test evaluates the hypothesis (there exists a significant difference between the average of these two groups). The text in red highlights the cases where the hypothesis was accepted, for a level of significance of 0.05. Moreover, the three decimals have been selected for a clear comparison. From the previous results, it means that the calibration proposed mainly corrects the average difference. It corroborates the assumption that StaMPS provided less fitted results than the other configurations and that the DSC direction needs higher calibration than the other configurations for PSI method. However, for QPS method ASC needs more calibration than DSC. It should be noted that from Table 7 (11 out of the 12) Welch's t-tests performed on the original InSAR configuration results showed a significant difference between the averages of the two groups (not passed the test). This demonstrates the need for calibration of the original results,

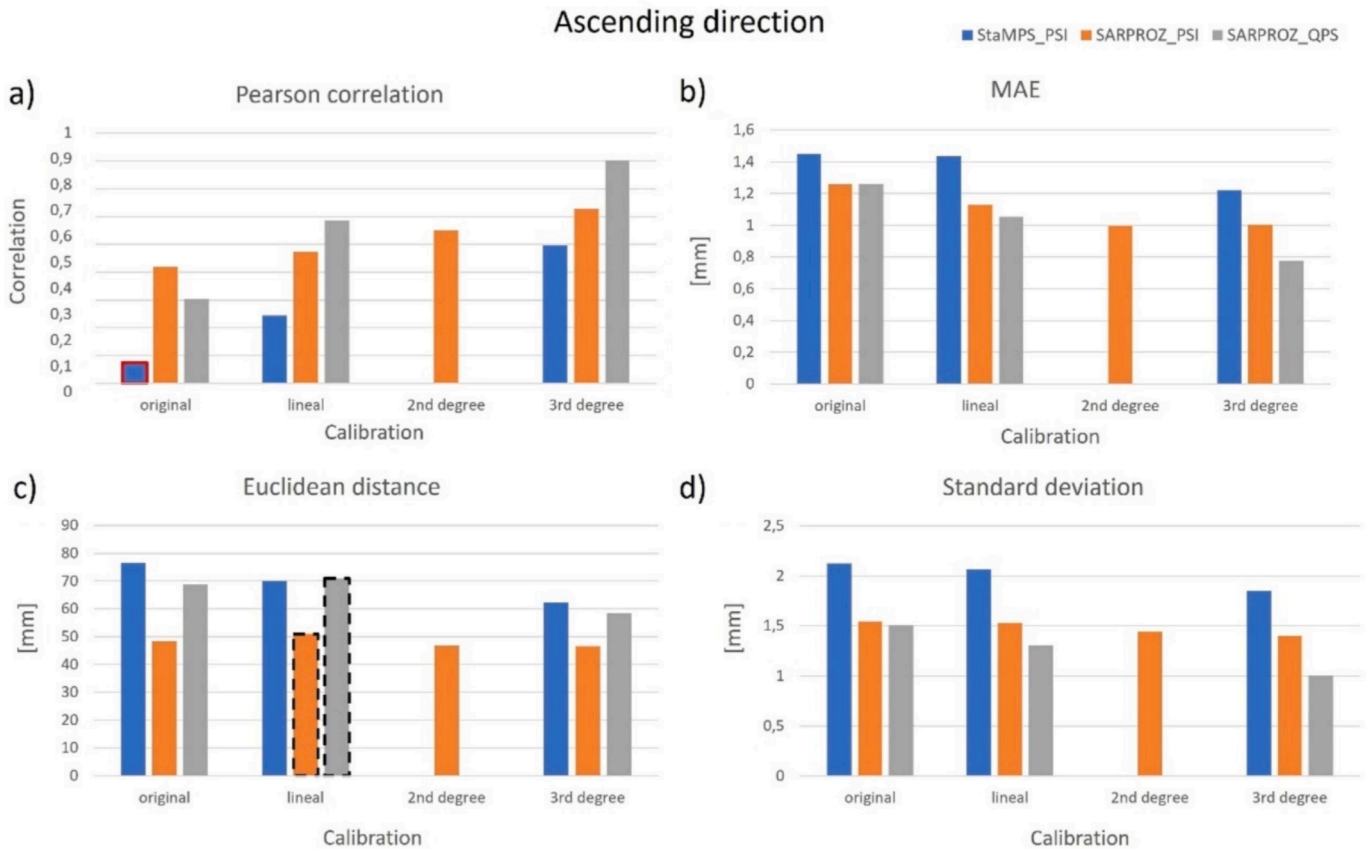


Fig. 8. Bar chart comparing the results for the ascending direction of the different calibrations proposed relative to the metrics (a) Pearson correlation; (b) MAE; (c) ED; and (d) SD.

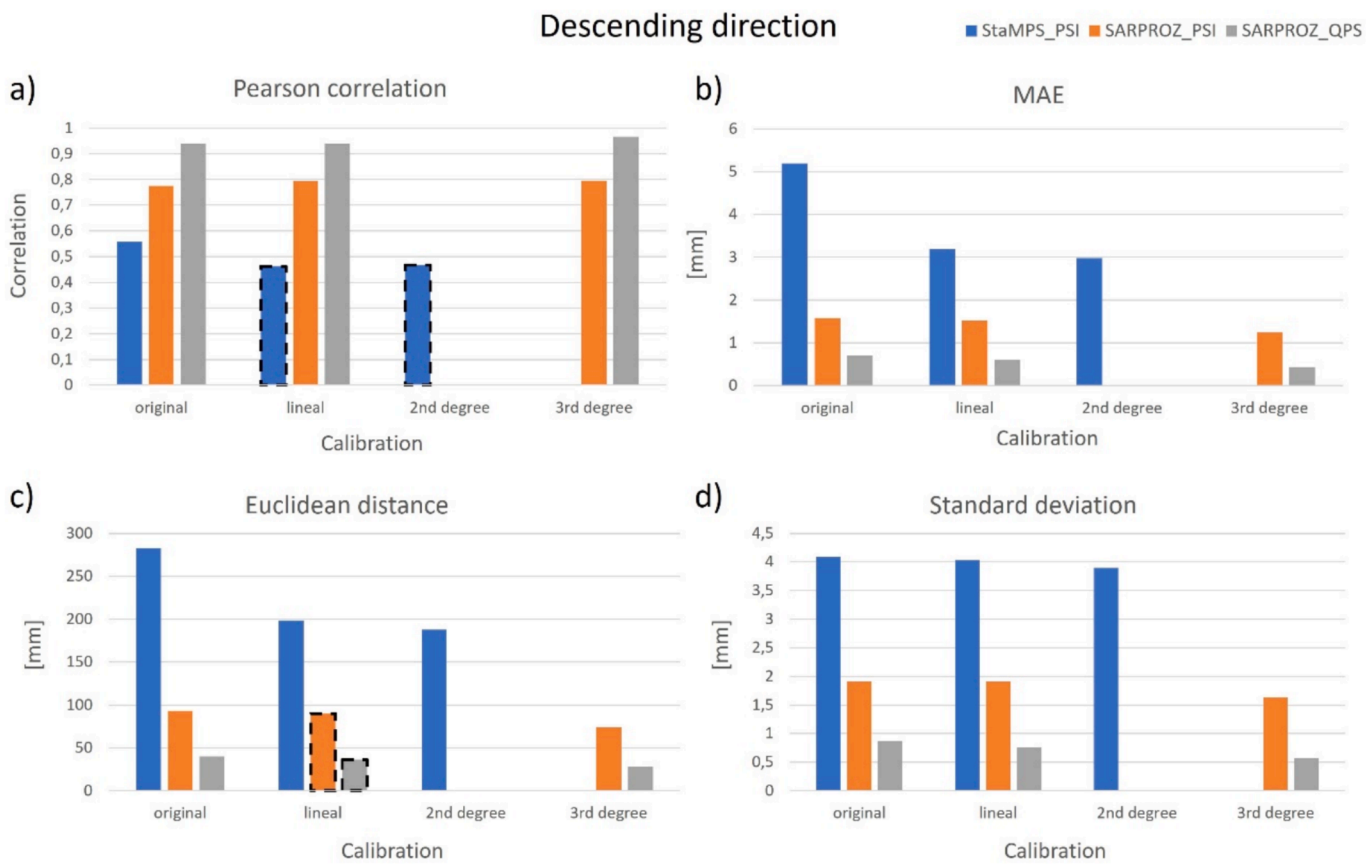


Fig. 9. Bar chart comparing the results for the descending direction of the different calibrations proposed relative to the metrics (a) Pearson correlation; (b) MAE; (c) ED; and (d) SD.

as previously conveyed in [6].

3.3. Validation of calibration procedure

After obtaining the possible calibrations, a two-level verification (local and global) was performed to assess whether the calibration improves the original InSAR results.

The local verification was performed between points A-C (Fig. 6), which represent the CRs installed in the LNEC complex (dCR and TTCR). In this case, comparisons could only be made in the vertical direction, as the TTCR installed in the west wing of the LNEC had been monitored using levelling technology (20 measurements). Fig. 12a shows the time series obtained with each configuration (StaMPS_PSI, SARPROZ_PSI and SARPROZ_QPS). One more time SARPROZ fits better to the ground-truth (levelling data) than StaMPS. Fig. 12b-d presents the original and calibrated time series for each configuration against the levelling data. At first glance, the calibrations seem reasonable, the one over StaMPS is the largest and most evident calibration because the original results are not that significant, and all of them may improve the initial time series.

To quantitatively analyze whether the calibrations truly enhance the original series, Fig. 13 compares the metrics, the evolution remarks that almost all the calibrations improve the original results. It is marked with black dashed contour the metrics with worse results than the original ones (in this case two metrics: Pearson correlation for the QPS with SARPROZ, and standard deviation for the PSI with SARPROZ).

Fig. 14 represents the evolution of the difference in the means of the data obtained with the different configurations in the vertical component between the CRs installed in the LNEC complex. The Welch *t*-test is performed for each case and is indicated with a red outline when the null hypothesis is not passed, indicating a significant difference between the groups. The improvement levels over the original values are similar for StaMPS, but not for SARPROZ.

The calibration showing the most significant evolution occurs in the case of StaMPS with the PSI method. The metrics that improve the most with calibration are average difference, MAE, and ED (in that order). Comparing the results from Fig. 10 with those of Fig. 13, the evolutionary trend appears similar. For example, the linear calibration on StaMPS_PSI in the MAE metric shows substantial improvement in both cases. However, two potential signs of overfitting can be identified in the SARPROZ results for the third-degree polynomial fitting (for PSI yielding better results than expected from the calibration results, and for QPS performing worse than anticipated). In SARPROZ_PSI, the relative improvement observed in the calibration area does not align with that seen in the local validation area (Fig. 10). Specifically, metrics such as Pearson correlation and Welch's *t*-test exhibit significantly better results in local validation than in calibration. Conversely, for SARPROZ_QPS, the performance deteriorates notably in the local validation area compared to the calibration, particularly in terms of Pearson correlation and Euclidean distance, suggesting another possible indication of overfitting.

In summary, this validation shows that StaMPS improves significantly with linear calibration, and it does not seem necessary to apply a more complex calibration as the improvement does not justify it. In the case of SARPROZ: i) for PSI, the most significant improvement is on the mean, passing the null hypothesis of the Welch's *t*-test (Fig. 14), thus this metric and Pearson justify that the third-degree adjustment is the best option; and ii) for QPS, the calibration also improves the original results, but in this case without passing the null hypothesis of the Welch's *t*-test (the linear adjust achieves the most based results).

The global validation is conducted between GNSS-monitored points separated by approximately 4 km. Points B and D in Fig. 6 represent the Gulbenkian buildings of the LNEC complex and the Direção Geral do

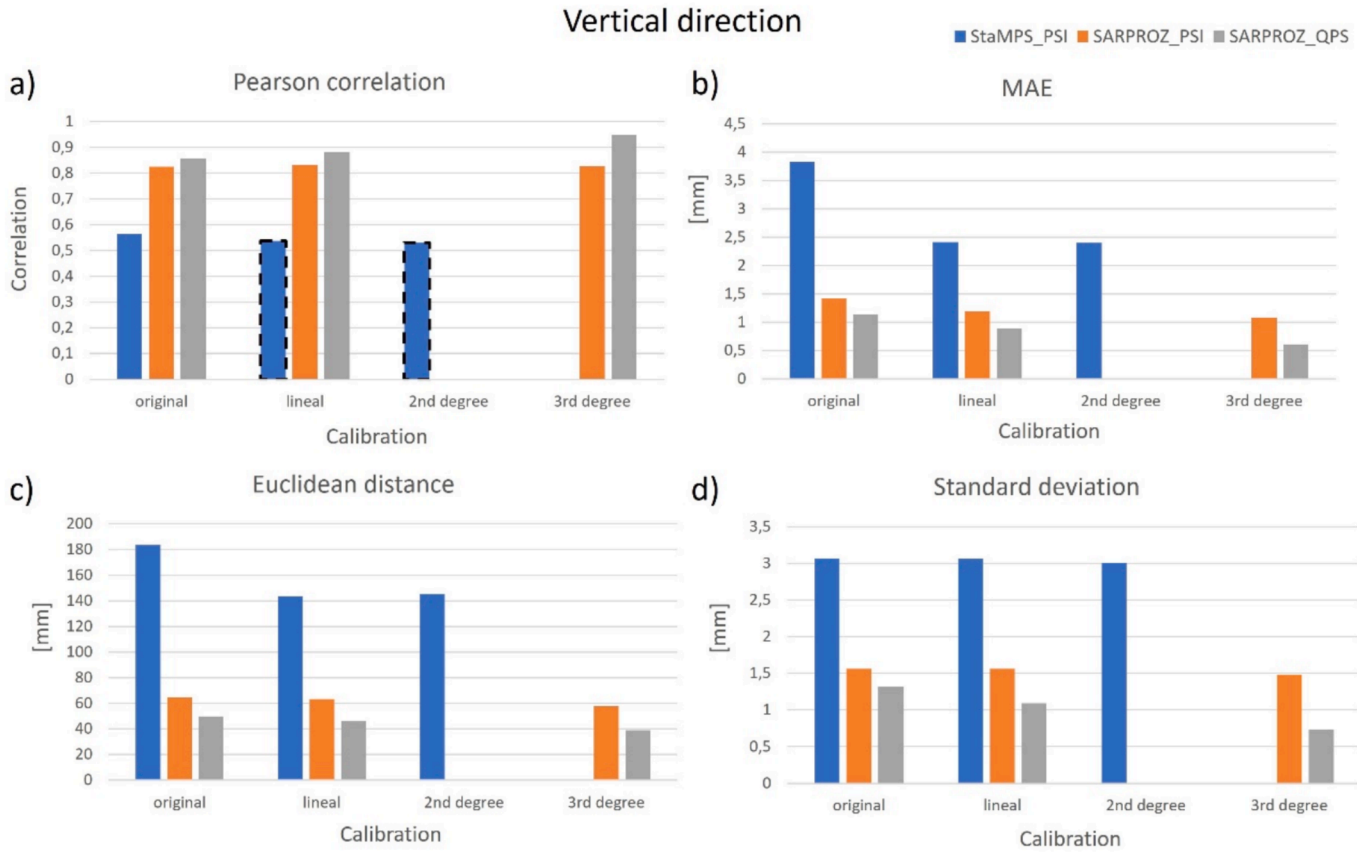


Fig. 10. Bar chart comparing the results for the vertical direction of the different calibrations proposed relative to the metrics (a) Pearson correlation; (b) MAE; (c) ED; and (d) SD.

Território, respectively. Since both are monitored by GNSS, the comparison can be made in the four directions under study (Ascending LOS, Descending LOS, vertical, and horizontal). This comparison allows for a more thorough analysis. Based on the results in Table 5, the precision of GNSS technology deteriorates (from submillimeter values to several millimeters) and the data exhibits greater dispersion. Consequently, the quantitative analysis becomes more complex and relative. For this reason, the analysis will focus on the metrics that are less affected by the increase in error and dispersion (mean and MAE analysis). The results are presented based on those obtained by each algorithm (StaMPS_PSI, SARPROZ_PSI and SARPROZ_QPS) for each direction in the following order (ASC, DSC, vert, hor). For each direction, the different time series obtained with each algorithm, along with their corrections, will be presented using the same color pattern (Figs. 15-18). After plotting the time series, the combined evolution of the metrics is shown to quantitatively support the analysis (Fig. 19).

Fig. 15 shows the time series obtained for each algorithm in the ASC LOS direction. In all three configurations, the time series appear to represent the same elements and are comparable. From the difference in scale, all results exhibit greater dispersion, with the results from StaMPS showing the highest variability. Considering the corrections, it is not visually recognizable whether they improve or worsen the results. However, observing Fig. 19a, the MAE metric does not present an evolution improvement like Fig. 8b, but shows slight improvements over the original values in the order (STAMPS_PSI, SARPROZ_PSI, and SARPROZ_QPS, respectively). Additionally, the average metric presents substantial improvements (evolving from failing Welch's *t*-test to passing it). Regarding StaMPS on the mean metric, although there still seems to be room for improvement, the third-degree adjustment passes Welch's *t*-test, making this calibration the best option. However, in Table 7, the implementation of this adjustment was not justified, as the linear adjustment was deemed sufficient. In the case of SARPROZ, the mean metric improvement is like in the LNEC calibration (Table 7), and the linear adjustment is enough. Hence, it is confirmed that the original results required correction (as they did not pass Welch's *t*-test) and that the calibration performed improved the original results (Fig. 19a).

Fig. 16 displays the results for the DSC LOS. In this case, the results from StaMPS_PSI and SARPROZ_PSI seem worse than those in the ASC direction (greater dispersion—Y-axis scale and adjustment to the ground-truth, respectively). For example, in the case of SARPROZ_PSI, the trend appears to be ascending, while according to GNSS, it is a flat trend. Regarding the corrections, in the case of StaMPS, the improvement is evident, but for SARPROZ_PSI and SARPROZ_QPS, the results improve in some parts and deteriorates in others.

However, reviewing the graphs in Fig. 19b, the mean test shows substantial improvement, being consistent with the results for the LNEC calibration (Table 7). MAE values for STAMPS_PSI improve significantly like in the LNEC calibration (Fig. 9b), for SARPROZ_PSI are small improvements also like in the LNEC calibration with similar evolution, and for SARPROZ_QPS is a slight worsening because the results are already satisfactory, but still not passing the Welch's *t*-test (in the LNEC calibration the evolution was a small improvement in MAE and mean analysis). Therefore, for this second case of global validation, it is also confirmed that the calibration improves the original results and that the best calibration over the three configurations is the linear adjustment, being consistent with the LNEC calibration where that calibration was the best-justified option.

Fig. 17 shows the results in the vertical direction. In this case, it is not evident that the time series from different configurations closely match the GNSS data, as the GNSS data exhibits significant dispersion, making it challenging to extract a clear trend. Visualizing the results from Fig. 19c, the MAE metric improves again with corrections, notably for

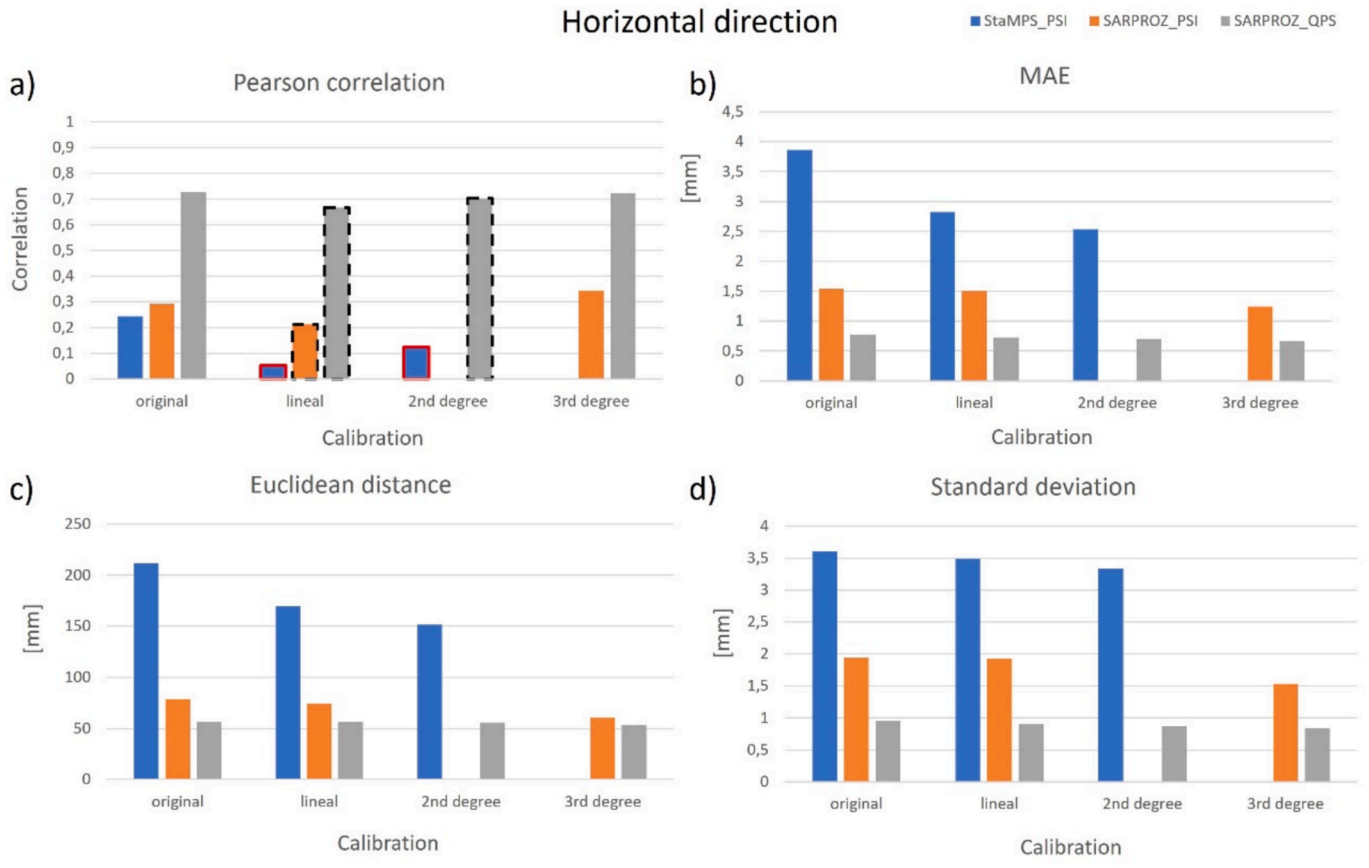


Fig. 11. Bar chart comparing the results for the horizontal direction of the different calibrations proposed relative to the metrics (a) Pearson correlation; (b) MAE; (c) ED; and (d) SD.

Table 7
Welch's *t*-test results for the mean difference between InSAR and GNSS observations over the different calibrations, directions and configurations proposed.

Welch's *t*-test	Ascending				Descending			
Means difference [mm]	Original	Linear	2nd degree	3rd degree	Original	Linear	2nd degree	3rd degree
StaMPS_PSI	0.541	0.002	–	0.002	4.863	0.023	0.023	–
SARPROZ_PSI	0.533	0.046	0.046	0.046	0.640	0.052	–	0.052
SARPROZ_QPS	0.547	0.030	–	0.031	0.206	0.015	–	0.015
	Vertical				Horizontal			
	Original	Linear	2nd degree	3rd degree	Original	Linear	2nd degree	3rd degree
StaMPS_PSI	3.571	0.012	0.012	–	3.244	0.021	0.021	–
SARPROZ_PSI	0.828	0.006	–	0.006	0.098	0.001	–	0.002
SARPROZ_QPS	0.569	0.010	–	0.010	0.267	0.038	0.038	0.038

STAMPS, but the changes for SARPROZ are insignificant. The mean test shows significant improvement for STAMPS and SARPROZ_QPS. However, for SARPROZ_PSI, it worsens although it still passes the Welch's *t*-test (based on that result, the calibration over SARPROZ_PSI is not justified). The warning signal suggesting that something unusual may be occurring in SARPROZ_PSI is that the original results pass the Welch's *t*-test outperforming those in the calibration area. This should not happen, given their higher baseline involves more components, which would typically lead to increased inaccuracy. The explanation for this odd situation is that while in the other cases, the common GNSS-InSAR points are representative of the total (similar averages), in this case, they are not, due to the noise in the GNSS observations. Applying Welch's *t*-test to the total dataset, the mean metric improves as in the other cases (from ~ 1 mm of average difference in the original results to ~ 0.2 mm after the calibration).

Analyzing the consistency between the results of the MAE and mean metrics for each configuration in the LNEC calibration, local validation, and global validation. The evolution in StaMPS is similar for MAE in the LNEC calibration (Fig. 10b) and local validation (Fig. 13b). Similarly, the evolution of the mean metric is also consistent (Table 7 for LNEC calibration and Fig. 14 for local validation). In all three cases, a linear fit is the best-justified option. For SARPROZ, this consensus is not present. For SARPROZ_PSI, global validation and LNEC calibration justify that the best calibration is the linear adjustment, while local validation justifies a third-degree adjustment (Fig. 14). A similar situation occurs with QPS_SARPROZ, where both validations (local and global) advocate for linear calibration, but the LNEC calibration for the MAE metric (Fig. 10b) suggests that the third-degree adjustment provides the best results, reinforcing our previous assumption that this indicates a sign of overfitting.

Fig. 18 shows the results for the horizontal component. The time series from STAMPS_PSI and SARPROZ_PSI appear comparable to the

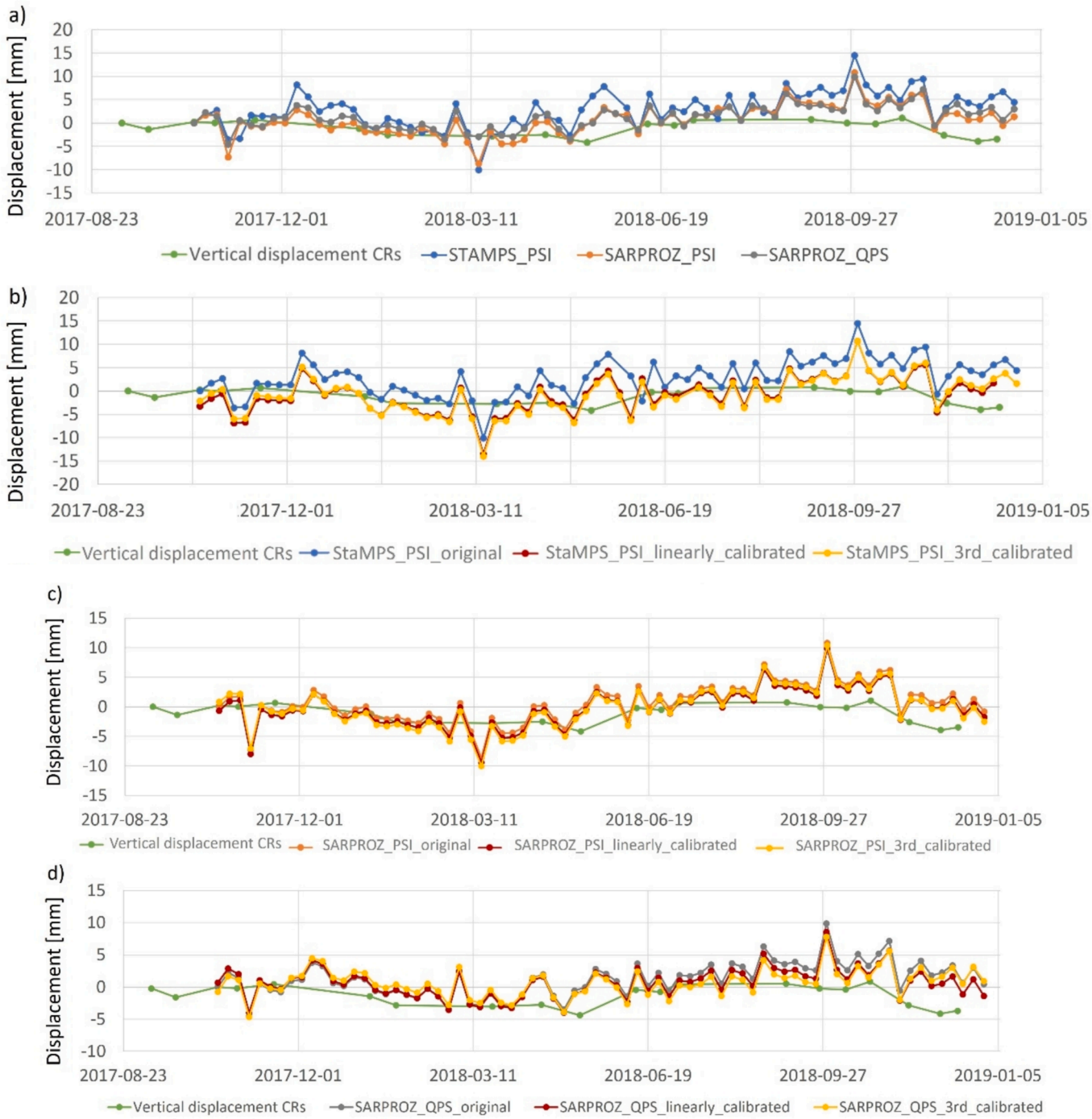


Fig. 12. Vertical displacement time-series results between the CRs installed in LNEC complex comparing (a) different configurations; (b) StaMPS PSI calibrations; (c) SARPROZ PSI calibrations; and (d) SARPROZ QPS calibrations.

GNSS data. In the case of SARPROZ_QPS, the trend and form differ. The corrections seem to improve the original series in all cases (Fig. 18). Reviewing Fig. 19d, the MAE metric supports the conclusion that StaMPS shows a significant improvement, meanwhile the enhancements in SARPROZ are comparatively smaller, this stems from the fact that the original results were already of remarkable quality, as indicated by the narrower Y-axis scale. Similarly, the mean metric improves with the corrections, even passing Welch's *t*-test for STAMPS_PSI.

Evaluating the consistency of evolution with the calibration results over the LNEC complex (Fig. 11b for MAE and Table 7 for mean metric). In the case of StaMPS and SARPROZ_QPS the evolution is comparable for both metrics, and the best-justified adjustment is the linear one. About SARPROZ_PSI the evolution differs between both metrics, because the third-degree correction provides better results over MAE metric and similar results than lineal calibration over the mean metric. Thus, while the third-degree adjustment produces the best results, the improvement rate may not be sufficient to justify the complexity of a third-degree function.

Since the vertical component is the most interesting in engineering due to its direct relation to problems like subsidence and sinkholes, the final analysis is conducted to evaluate which option provides better results: i) Calibrating the original data in the LOS and then converting it

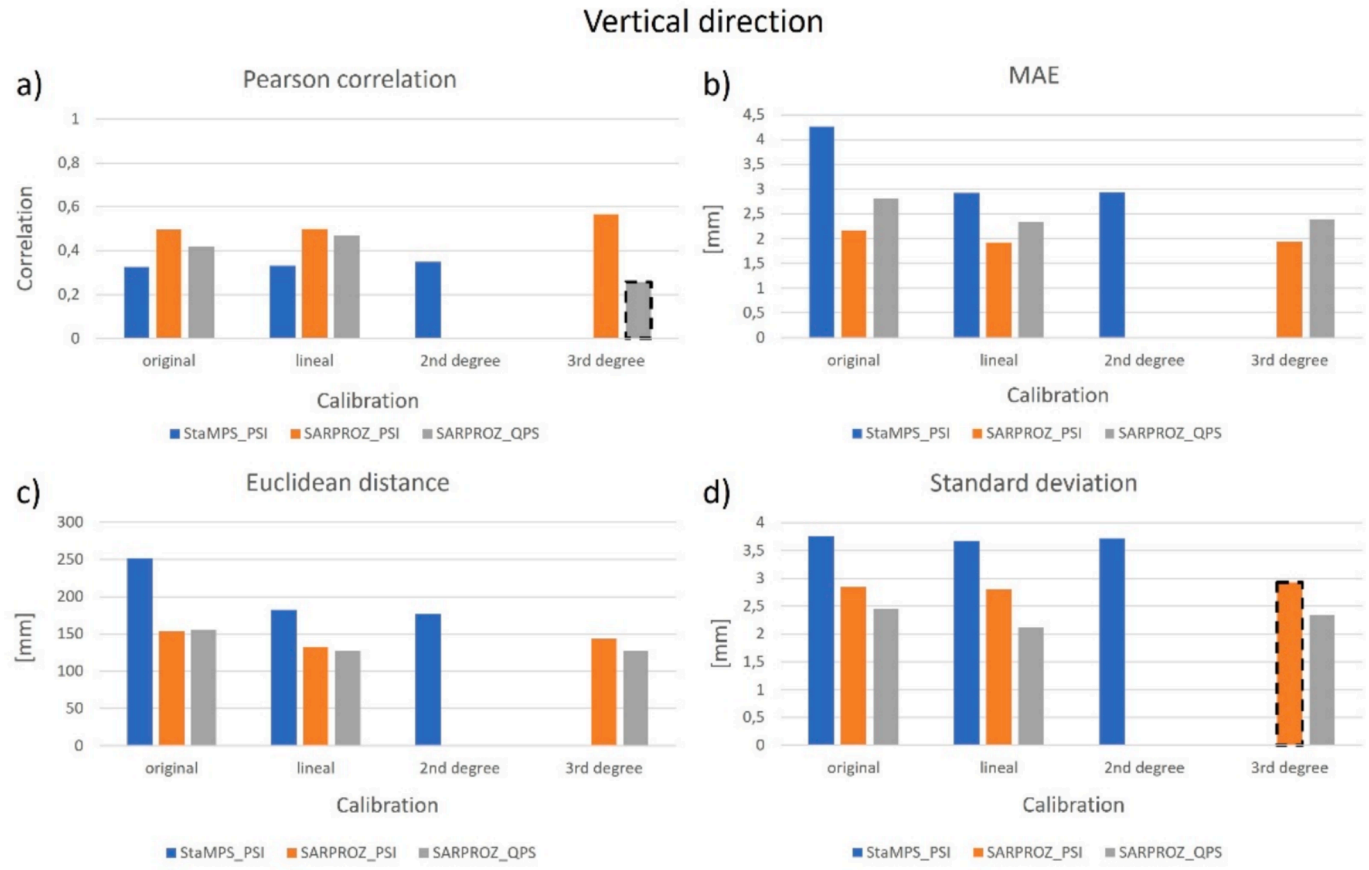


Fig. 13. Evolution of the different calibrations metrics for vertical direction between the CRs installed in LNEC (a) Pearson correlation; (b) MAE; (c) ED; and standard deviation.

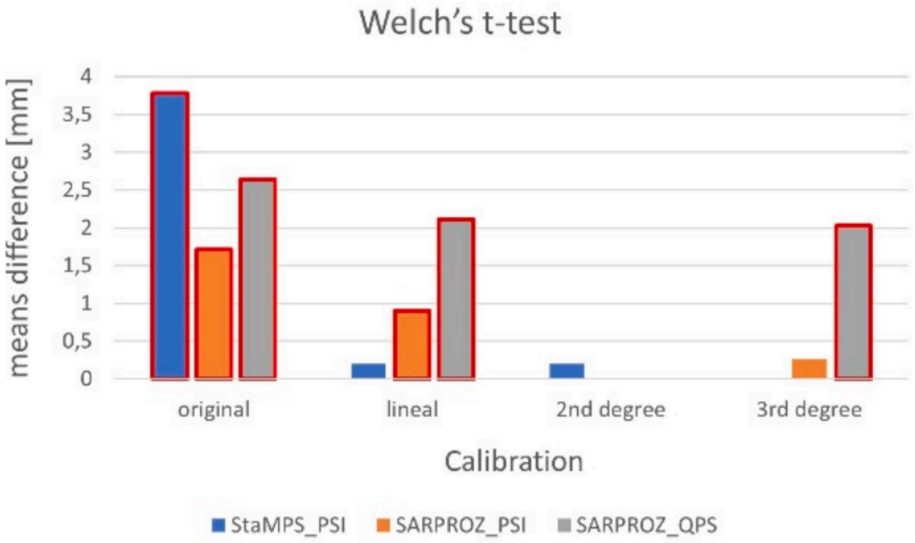


Fig. 14. Evolution of the mean difference for vertical direction between the CRs installed in LNEC for the different configurations.

to vertical, or ii) Performing a specific calibration on the vertical component as shown in Fig. 7C, 12 and 17. This evaluation aims to identify the most effective calibration approach for addressing engineering-related vertical displacement issues. As shown in Fig. A2 and Table A2 (in Appendix A), the results from both approaches are similar and differ under the millimeter. About the average difference analysis: for StaMPS_PSI performing a custom calibration on the Ascending and Descending time series provides better results on average metric; and for SARPROZ_QPS the direct calibration over vertical component achieves more accurate outcomes. However, although the MAE metric is marginally lower for the first approach (calibrating the original LOS data prior to vertical conversion), the additional time and effort required may not be justified by the relatively small improvement.

Table 8 presents the best-justified adjustment, with the linear

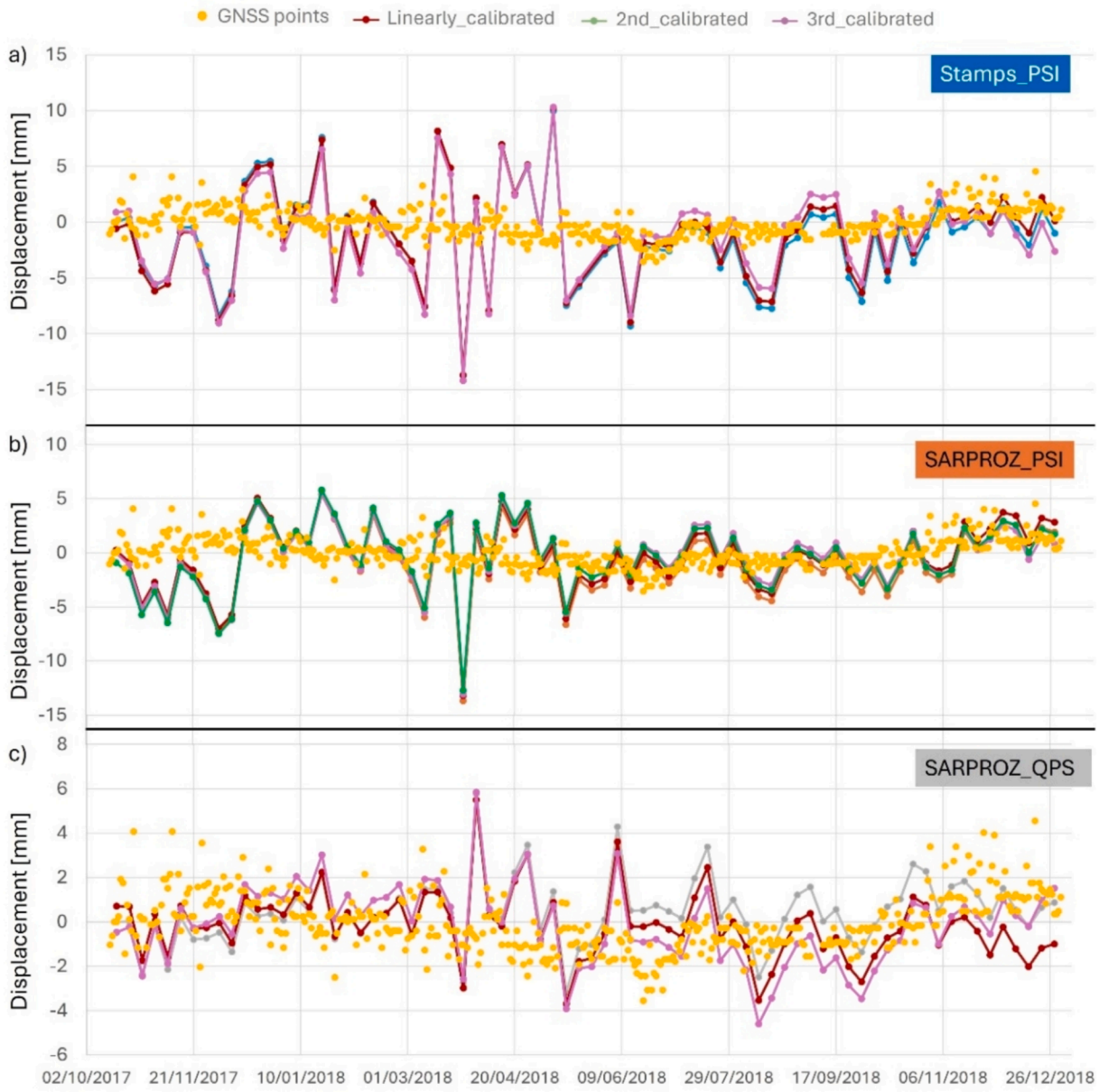


Fig. 15. Time series for the ascending direction comparing the results obtained with each InSAR configuration, the purposed corrections, and GNSS between the monitored buildings Gulbenkian and Direção Geral do Território. a) StaMPS_PSI, b) SARPROZ_PSI, and c) SARPROZ_QPS.

calibration (consistently improving the results across all configurations) emerging as the most reliable and broadly applicable approach. However, more complex adjustments (e.g., second-degree polynomial) offered marginal improvements in specific cases, suggesting a trade-off between model complexity and generalizability.

3.4. Limitations and future considerations

The limitations that must be considered when applying it in different contexts are:

i) On the GNSS side, the main constraint is achieving high-precision positioning, which depends on factors such as measurement frequency, signal quality, and satellite coverage (communication with sufficient number of satellites). Ensuring continuous, high-quality GNSS data acquisition remains a challenge, particularly in areas with obstructed sky visibility or limited infrastructure. The proximity between GNSS stations is crucial for achieving high-precision relative positioning. Therefore, in the absence of nearby antennas from permanent GNSS networks, a temporary antenna operating continuously during the monitoring period can be used as an effective alternative.

ii) Regarding InSAR, the method requires the availability of complementary SAR acquisitions with suitable temporal and geometric baselines. These are essential for compensating LOS deformation and enabling the decomposition of displacements into vertical and horizontal components. Without access to diverse acquisition geometries, deformation analysis may be restricted to the LOS direction, limiting interpretability in many monitoring scenarios.

iii) The CR must be precisely located (open area), and correctly oriented and adapted with respect to the SAR sensor to ensure consistent radar backscatter throughout the observation period (the CR used in the research was specific for Sentincel-1 SAR products). For other sensors the CR must be adapted to fit the size and orientation. Furthermore, both the CR and the co-located

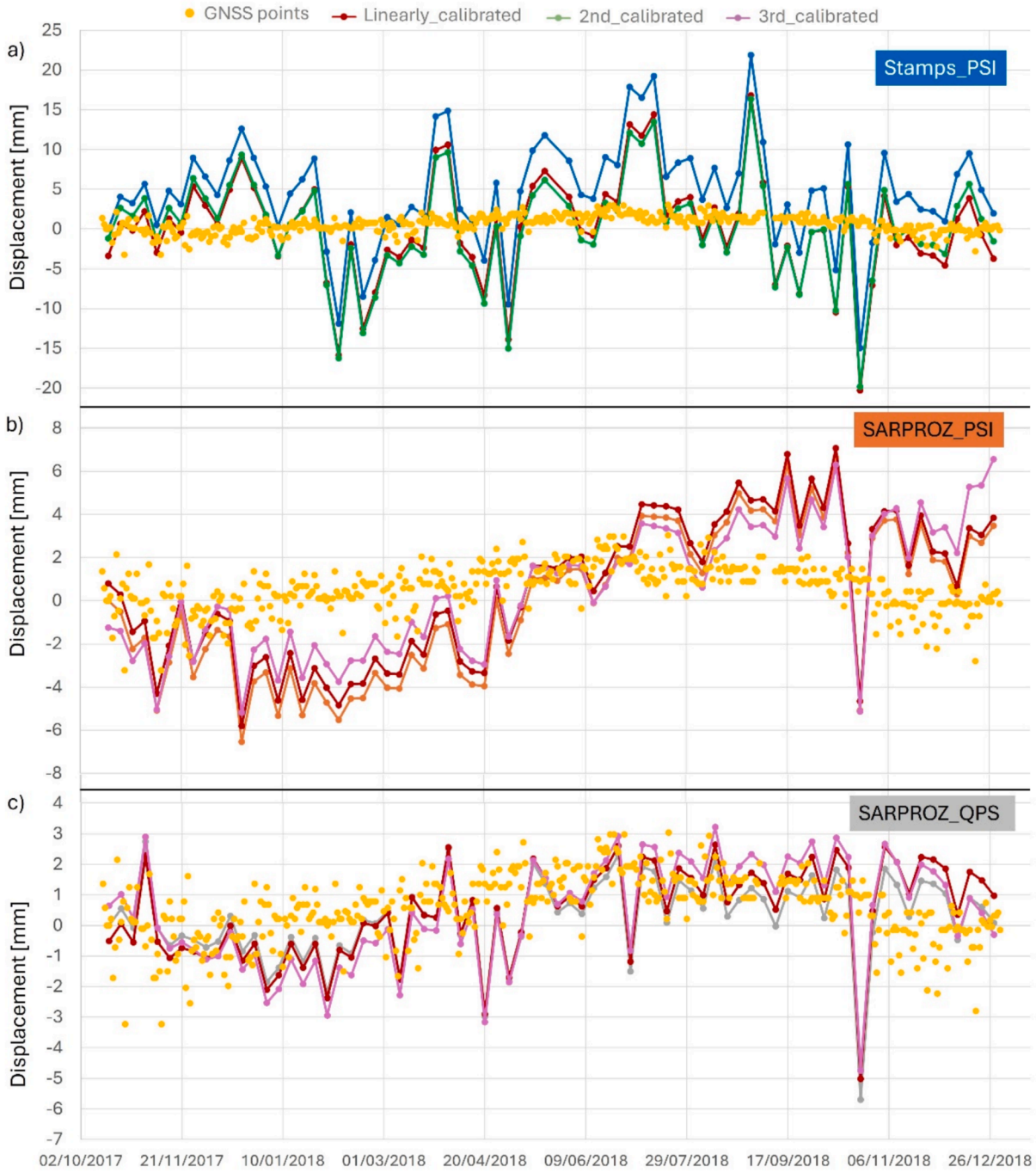


Fig. 16. Time series for the descending direction comparing the results obtained with each InSAR configuration, the purposed corrections, and GNSS between the monitored buildings Gulbenkian and Direção Geral do Território. a) StaMPS_PSI, b) SARPROZ_PSI, and c) SARPROZ_QPS.

GNSS antenna must be regularly monitored to verify the absence of any exceptional events (e.g., physical disturbance, obstruction, or malfunction) that could compromise the stability or validity of the measurements.

iv) Site conditions impose additional constraints. The calibration approach requires that the surrounding area includes coherent elements suitable for consistent InSAR analysis. Sudden or irregular ground movements in the vicinity—such as landslides, heavy construction, or unstable terrain—can affect phase stability and hinder the identification of reliable reference points. Similarly, GNSS performance may be degraded in areas with poor satellite visibility or limited data transmission capabilities.

The proposed method will contribute to promoting the usage of InSAR displacements for structure monitoring. InSAR displacement uncertainty is slightly larger than that usually achieved for structure monitoring through in-situ methods. Therefore, the proposed calibration will be a valuable contribution, by reducing InSAR displacement uncertainty. Future research should develop methods to validate calibration effectiveness at other elements apart from structures—particularly in interurban or vegetated areas where GNSS infrastructure is sparse—would greatly enhance the applicability of the technique. The possibility of generalizing the calibration approach would be important to reduce the dependence on specific control points. It can be done with temporal GNSS stations, but it is costly and may not provide consistent InSAR scatterers. For that reason, it would be advisable to evaluate the

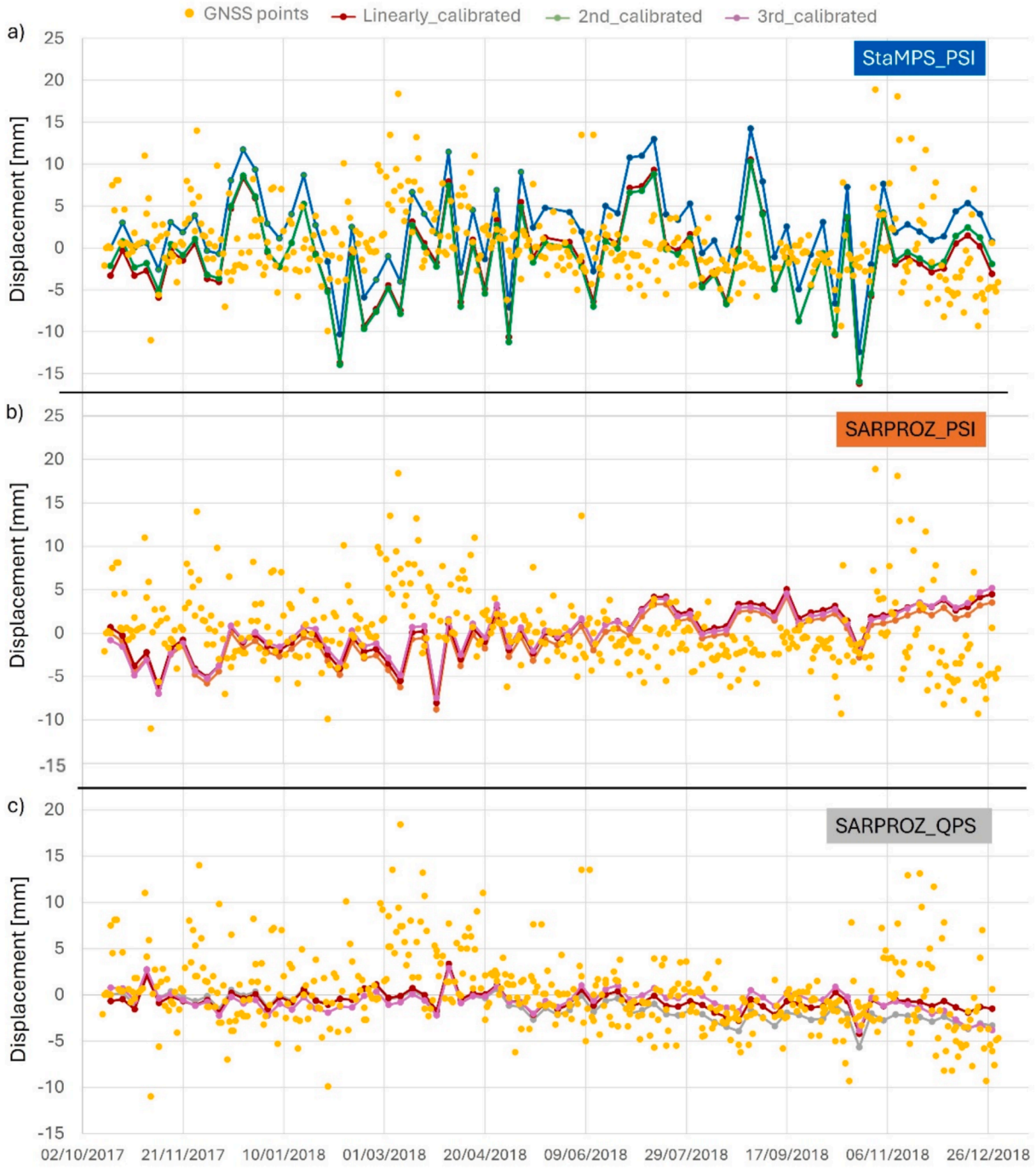


Fig. 17. Time series for the vertical direction comparing the results obtained with each InSAR configuration, the purposed corrections, and GNSS between the monitored buildings Gulbenkian and Direção Geral do Território. a) StaMPS_PSI, b) SARPROZ_PSI, and c) SARPROZ_QPS.

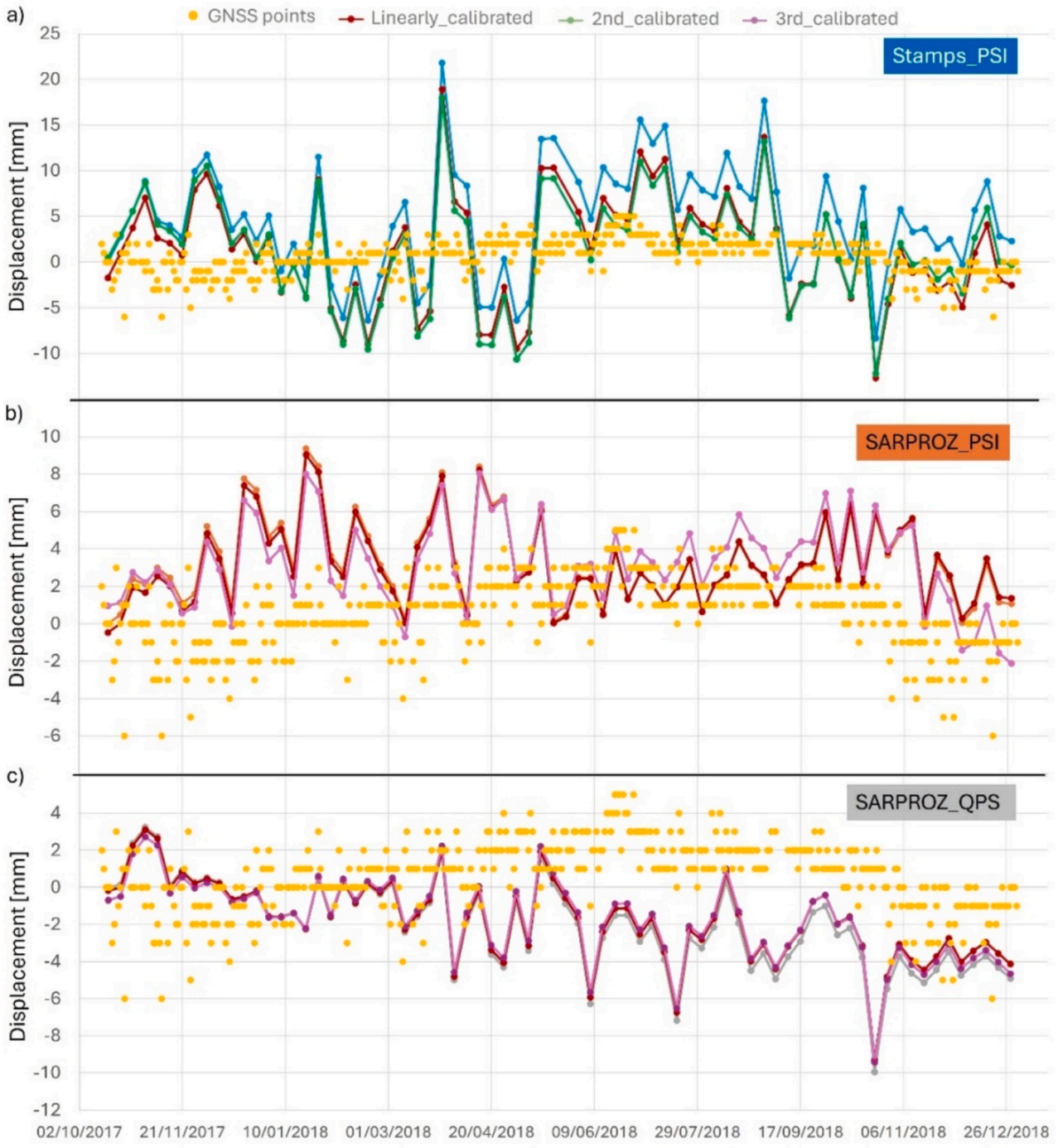


Fig. 18. Time series for the horizontal direction comparing the results obtained with each InSAR configuration, the purposed corrections, and GNSS between the monitored buildings Gulbenkian and Direção Geral do Território. a) StaMPS_PSI, b) SARPROZ_PSI, and c) SARPROZ_QPS.

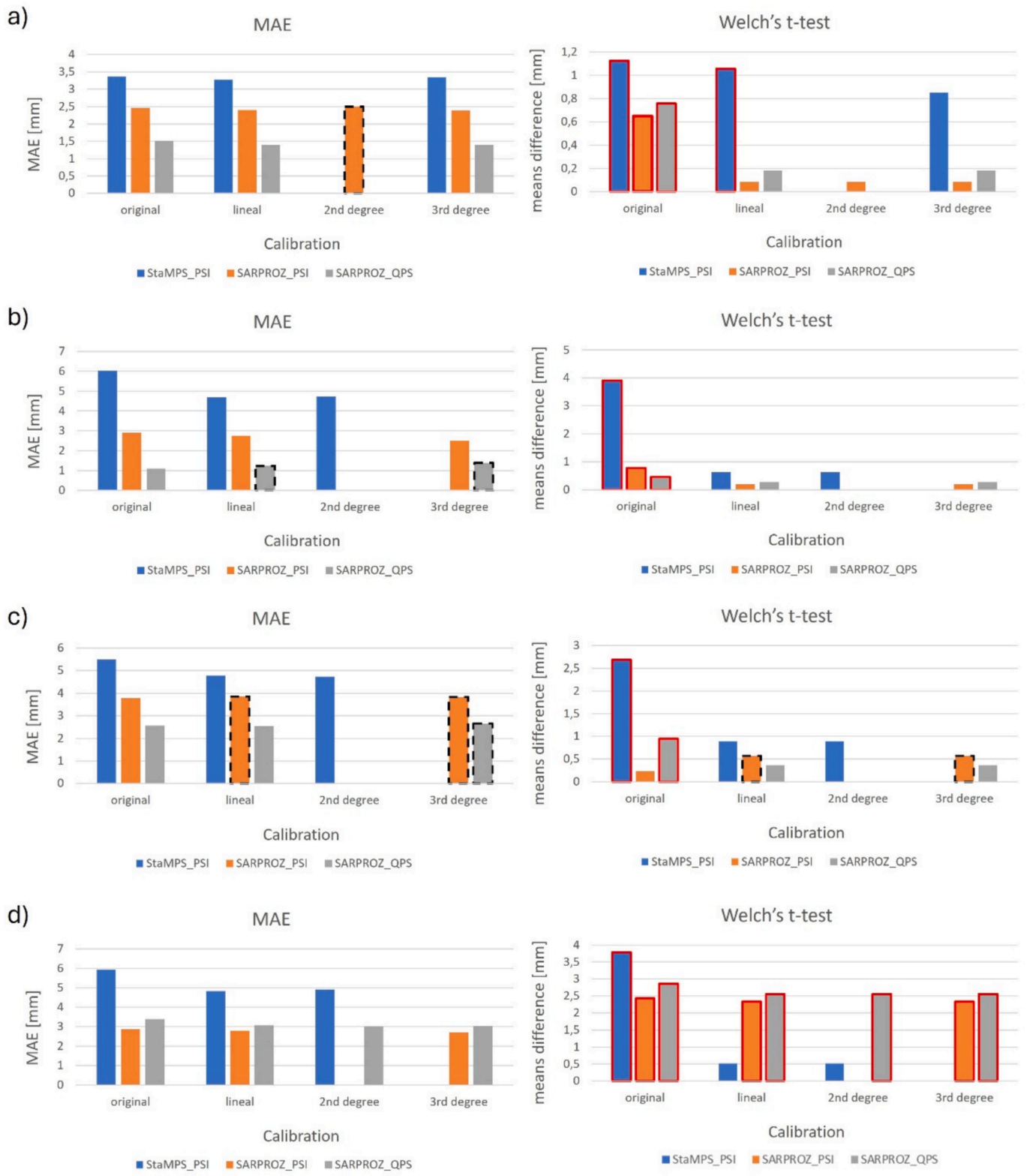


Fig. 19. Evolution of the metrics MAE and mean difference for the different configurations between the monitored buildings Gulbenkian and Direção Geral do Território for the directions, a) Ascending, b) Descending, c) Vertical, and d) Horizontal.

use of active artificial SAR reflectors like radar transponders. In order to apply the proposed method over large-scale areas or in remote regions, non-negligible atmospheric effects must be considered. In that case, atmospheric models may be used to mitigate those effects. Moreover, exploring strategies to implement the calibration framework across medium to large spatial extents, possibly through the creation of a model to streamline the correction process, integrating with atmospheric models, network-based adjustment techniques, spatial interpolation methods, or even directly to all data points. The validation of the application method will be essential for scaling the methodology and adapting it to regional or national deformation monitoring programs.

Table 8
Best-justify adjustment option for each direction, configuration and area.

	StaMPS_PSI			SARPROZ_PSI			SARPROZ_QPS		
	LNEC calibration	Local validation	Global validation	LNEC calibration	Local validation	Global validation	LNEC calibration	Local validation	Global validation
Ascending	3rd degree	–	3rd degree	Linear (2nd degree)*	–	Linear	Linear (3rd degree)	–	Linear
Descending	Linear	–	Linear	Linear (3rd degree)	–	Linear	Linear (3rd degree)	–	Linear
Vertical	Linear	Linear	Linear	Linear	Linear/ 3rd degree	Not justified	Linear (3rd degree)	Linear	Linear
Horizontal	Linear	–	Linear	3rd degree	–	Linear	Linear	–	Linear

* The best-performing results are shown in parentheses.

4. Conclusions

This study proposed and evaluated a GNSS-based calibration methodology over stable control points for InSAR displacement time series, using six case studies with varying configurations in software (StaMPS and SARPROZ), methods (PSI and QPS), and orbit directions (ascending and descending). InSAR measurement points were achieved in key locations of infrastructures, demonstrating that even under cases of lower standard coherence (less restrictive processing over StaMPS), reliable results are obtained with the proposed calibration method based on GNSS and CR.

The calibration was grounded on the time series comparison between InSAR-derived displacements and high-precision converted GNSS and levelling measurements at shared ground control points (CRs and buildings). Error time series were modeled using polynomial regressions as potential calibration functions. To evaluate the results, a statistical analysis was performed to report on trends, means, and errors. This combined analysis allows for an understanding of the adjustments' effects associated with their evolution. Based on these calibration functions, two types of validation were performed (local and global). The validation at a local level was conducted on the vertical component at a baseline of approximately 400 m, using levelling technology as the ground truth that monitored the displacement between TTCR and dCR for collecting the time series. The validation at a global level was performed in multiple directions (ascending LOS, descending LOS, vertical, and horizontal) because the comparison was made working with GNSS data between IGP0 GNSS station and Gulbenkian building (baseline of approximately 4 km).

The results demonstrate that original InSAR products require calibration: 25 out of 27 time series Welch's *t*-test exhibited statistically significant biases in their original form. Moreover, the calibration improved the original results (on both validations) reducing these biases (evidenced by the improvement in Welch's *t*-test results) and improved the overall error MAE metric, particularly in products generated with the StaMPS software, which showed higher variability and greater deviation from ground truth. SARPROZ products, especially those processed with the QPS method, displayed lower dispersion (not detecting the seasonal component), but also benefited from calibration.

Finally, it has to be mentioned that a direct calibration on the vertical component proved to be more efficient and practical than an individual calibration over ascending and descending time series prior to projection. Furthermore, the degree of improvement varied depending on the method and orbit, with reduced improvement index for the global validation in the cases of (StaMPS_PSI and SARPROZ_PSI), and with notably better performance in global validation for SARPROZ_QPS. These findings highlight the importance of integrating ground-based observations with stable control points to enhance InSAR accuracy and support operational monitoring applications.

CRediT authorship contribution statement

Alex Alonso-Díaz: Writing – review & editing, Writing – original draft, Visualization, Validation, Supervision, Software, Resources, Project administration, Methodology, Investigation, Funding acquisition, Formal analysis, Data curation, Conceptualization. **Dora Roque:** Writing – review & editing, Validation, Supervision, Resources, Project administration, Methodology, Formal analysis, Data curation, Conceptualization. **José Nuno Lima:** Writing – review & editing, Resources, Data curation. **Juan Luis Rodríguez:** Writing – review & editing, Supervision. **Mercedes Solla:** Writing – review & editing, Funding acquisition, Conceptualization.

Declaration of competing interest

The authors declare the following financial interests/personal relationships which may be considered as potential competing interests: This work has received funding from the STRADAR project (TED2021-130183B-I00), funded by MICIU/AEI/https://doi.org/10.13039/501100011033 and by the "European Union NextGenerationEU/PRTR". A. Alonso-Díaz acknowledges the funding received from the Xunta de Galicia through the project ENDITÍ (ED431F 2021/08), and the grant for stays in research centers "Axudas propias para a mobilidade de Persoal Investigador da UVigo (MOBVIGO_23)" from Universidade de Vigo. M. Solla acknowledges the Grant RYC2019–026604–I funded by MICIU/AEI/https://doi.org/10.13039/501100011033 and by "ESF Investing in your future". The authors would like to acknowledge Daniele Perissin (RASER Limited) for support with SARPROZ software, João Catalão (University of Lisbon) for support with the triangular trihedral corner reflector, Direção Geral do Território for the ReNEP data and the Canadian Geodetic Survey of Natural Resources Canada for the access to the CSRS-PPP service.

Acknowledgements

This work has received funding from the STRADAR project (TED2021-130183B-I00), funded by MICIU/AEI/10.13039/501100011033 and by the "European Union NextGenerationEU/PRTR". A. Alonso-Díaz acknowledges the funding received from the Xunta de Galicia through the project ENDITÍ (ED431F 2021/08), and the grant for stays in research centers "Axudas propias para a mobilidade de Persoal Investigador da UVigo (MOBVIGO_23)" from Universidade de Vigo. M. Solla acknowledges the Grant RYC2019–026604–I funded by MICIU/AEI/10.13039/501100011033 and by "ESF Investing in your future". The authors would like to acknowledge Daniele Perissin (RASER Limited) for support with SARPROZ software, João Catalão (University of Lisbon) for support with the triangular trihedral corner reflector, Direção Geral do Território for the ReNEP data and the Canadian Geodetic Survey of Natural Resources Canada for the access to the CSRS-PPP service. Funding for open access charge: Universidade de Vigo/CISUG.

Appendix

Table A1
Statistical results for the relative displacement between CR and Gulbenkian building in LNEC monitored by GNSS for the different configurations.

		Ascending			Descending			Vertical			Horizontal		
		PSI		QPS	PSI		QPS	PSI		QPS	PSI		QPS
		SM	SP	SP	SM	SP	SP	SM	SP	SP	SM	SP	SP
Tendency	Pearson	0.07	0.42	0.30	0.56	0.77	0.94	0.56	0.82	0.86	0.24	0.29	0.73
Average [mm]	t-Welch	0.54	0.53	0.55	4.86	0.64	0.21	3.57	0.83	0.57	3.24	0.09	0.27
Errors [mm]	MAE	1.45	1.26	1.26	5.19	1.58	0.70	3.83	1.42	1.13	3.87	1.54	0.78
	ED	76.64	48.45	68.77	282.79	93.18	39.67	183.49	64.52	49.86	211.29	78.80	56.78
	Standard deviation	2.12	1.54	1.51	4.09	1.91	0.87	3.06	1.56	1.31	3.61	1.94	0.95

*Where. SM means StaMPS and SP SARPROZ.
**In red are the results that rejected the significance hypothesis relative to the p_value.
***The results have two decimals to present the overall differences.

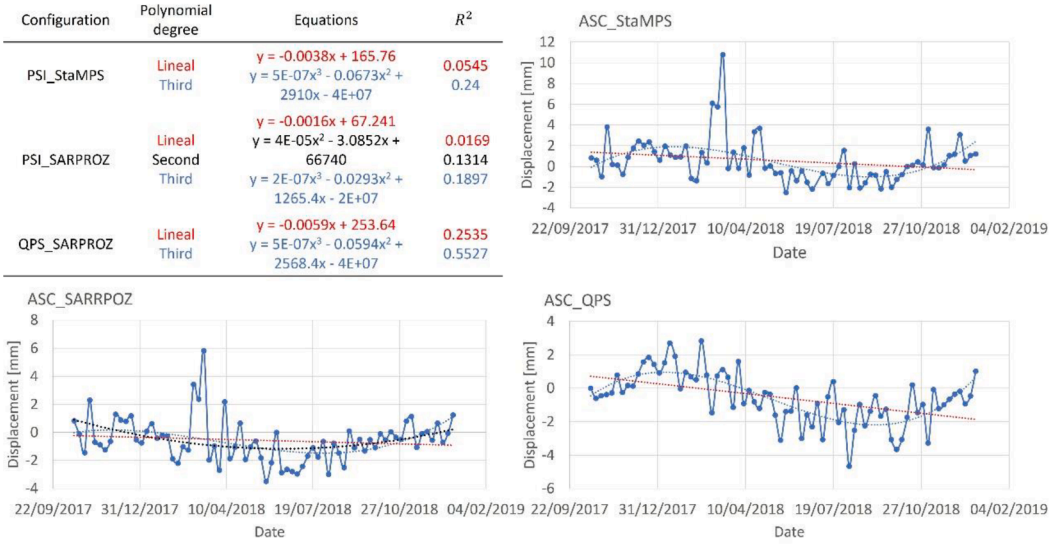
Table A2
Statistical results comparing the results over each algorithm between correction over the vertical component or over the ASC DSC LOS.

		StaMPS_PSI		SARPROZ_PSI				SARPROZ_QPS			
		Lineal Vertical	Linear ASC-DSC	Linear Vert	Linear ASC-DSC	3rd Vert	3rd ASC-DSC	Linear Vert	linear ASC-DSC	3rd Vert	3rd ASC-DSC
Average [mm]	t-Welch	0.8967	0.2741	0.5749	0.5746	0.4926	0.4925	0.3662	0.6230	0.3658	0.6152
Errors [mm]	MAE	4.7769	4.7137	3.8602	3.8222	3.8238	3.7868	2.9401	2.8323	2.6498	2.5526

*The results have four decimals to present the overall differences.
**In red are the results that rejected the significance hypothesis relative to the p_value.

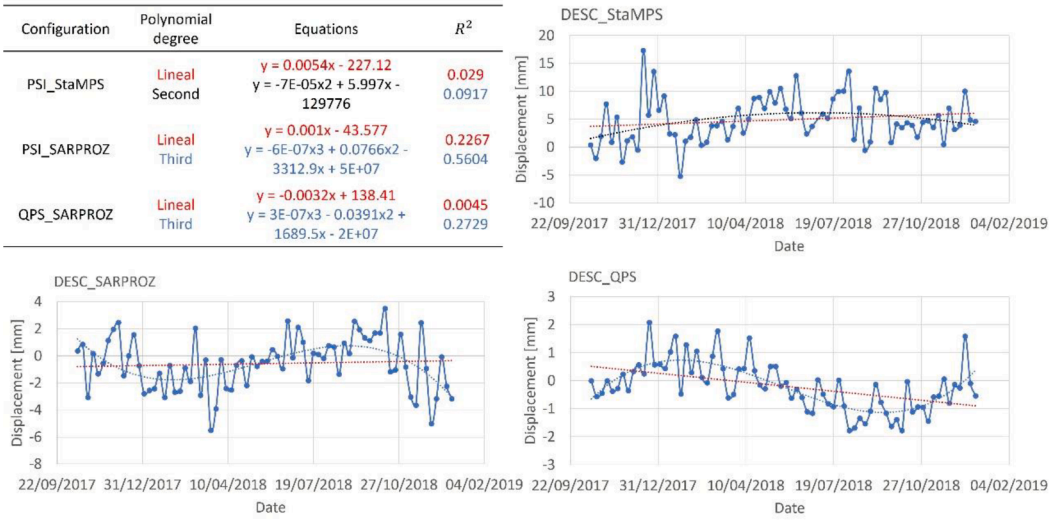
a)

Configuration	Polynomial degree	Equations	R^2
PSI_StaMPS	Lineal	y = -0.0038x + 165.76	0.0545
	Third	y = 5E-07x³ - 0.0673x² + 2910x - 4E+07	0.24
PSI_SARPROZ	Lineal	y = -0.0016x + 67.241	0.0169
	Second	y = 4E-05x² - 3.0852x + 66740	0.1314
	Third	y = 2E-07x³ - 0.0293x² + 1265.4x - 2E+07	0.1897
QPS_SARPROZ	Lineal	y = -0.0059x + 253.64	0.2535
	Third	y = 5E-07x³ - 0.0594x² + 2568.4x - 4E+07	0.5527



b)

Configuration	Polynomial degree	Equations	R^2
PSI_StaMPS	Lineal	y = 0.0054x - 227.12	0.029
	Second	y = -7E-05x2 + 5.997x - 129776	0.0917
PSI_SARPROZ	Lineal	y = 0.001x - 43.577	0.2267
	Third	y = -6E-07x3 + 0.0766x2 - 3312.9x + 5E+07	0.5604
QPS_SARPROZ	Lineal	y = -0.0032x + 138.41	0.0045
	Third	y = 3E-07x3 - 0.0391x2 + 1689.5x - 2E+07	0.2729



c)

Configuration	Polynomial degree	Equations	R^2
PSI_StaMPS	Lineal	y = 0.0013x – 54.486	0.0032
	Second	y = -4E-05x2 + 3.2102x – 69435	0.0353
PSI_SARPROZ	Lineal	y = -0.0006x + 24.626	0.0024
	Third	y = -3E-07x3 + 0.0358x2 – 1550.2x + 2E+07	0.1034
QPS_SARPROZ	Lineal	y = -0.0057x + 246.27	0.3144
	Third	y = 5E-07x3 - 0,0604x2 + 2609.9x - 4E+07	0.6851

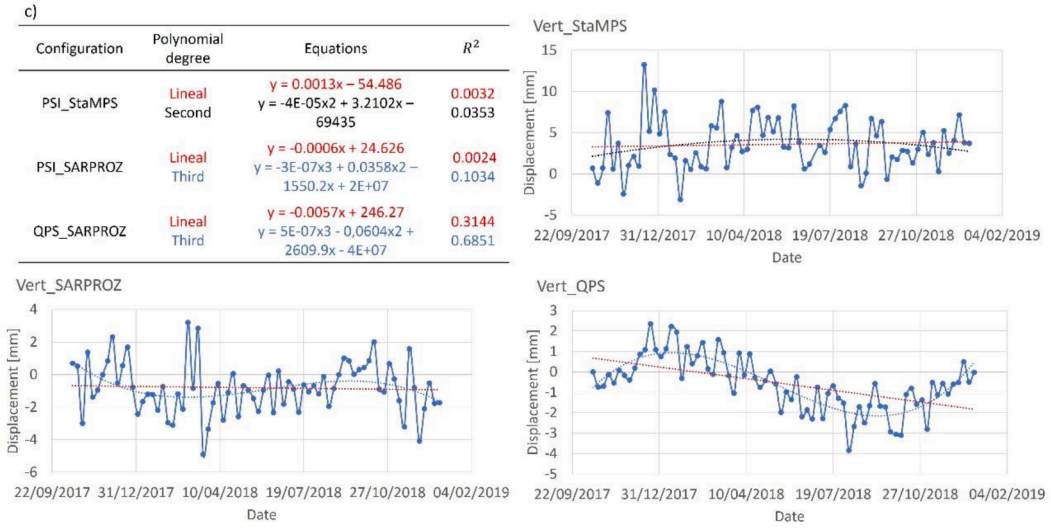


Fig. A1. Calibrations proposed for the different configurations for (a) Ascending; (b) Descending; (c) Vertical; and (d) Horizontal directions.

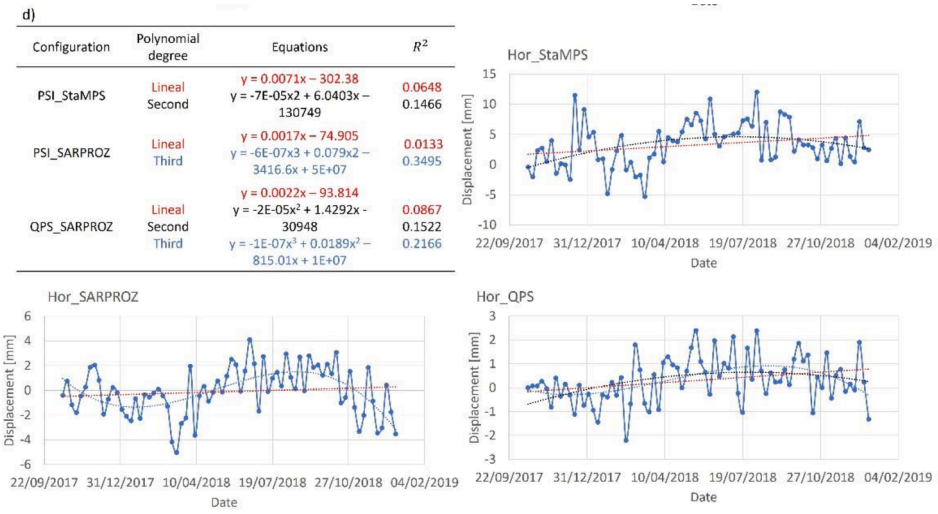


Fig. A1. Calibrations proposed for the different configurations for (a) Ascending; (b) Descending; (c) Vertical; and (d) Horizontal directions.

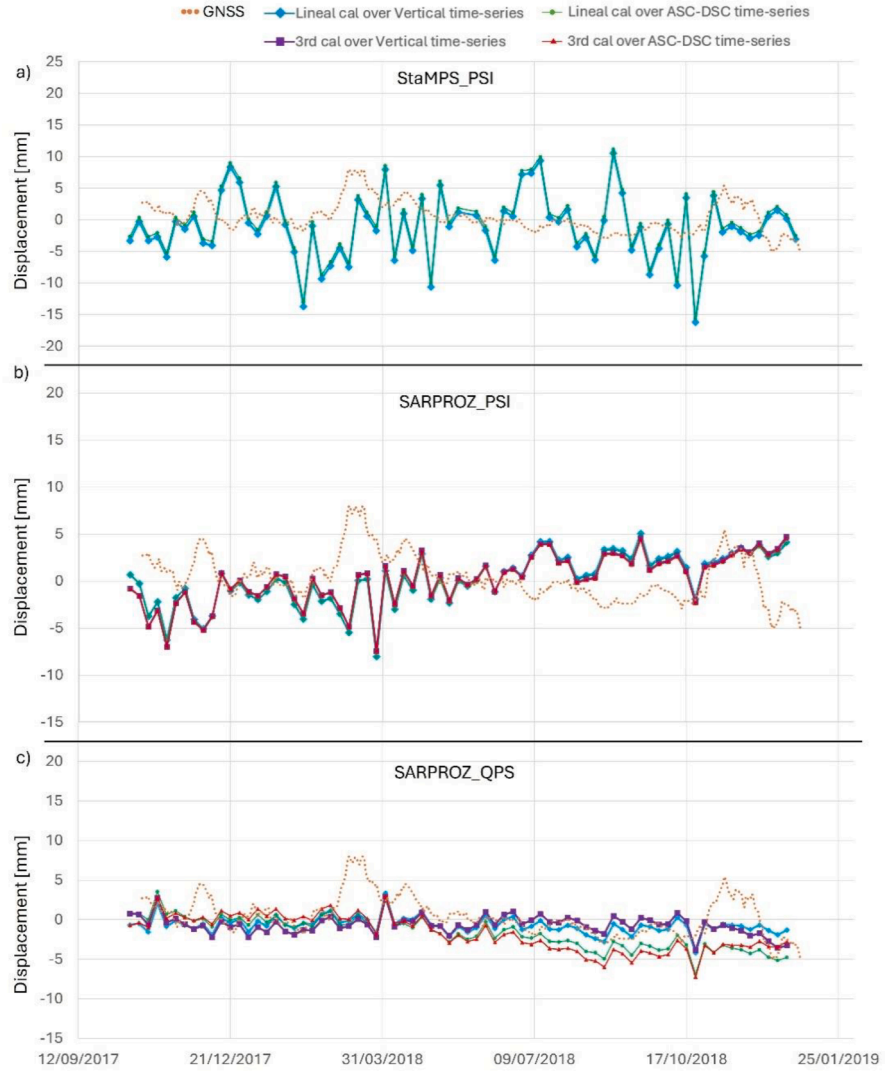


Fig. A2. Time-series obtained for the different corrections comparing adjustments directly over vertical component and over ASC and DSC LOS for (a) StaMPS_PSI; (b) SARPROZ_PSI; and (c) SARPROZ_QPS. *GNSS represented with 12-day moving average

Data availability

The authors do not have permission to share data.

References

[1] M. Mahdavifard, S. Kaviani Ahangar, B. Feizizadeh, K.K. Valizadeh, Spatio-Temporal monitoring of Qeshm mangrove forests through machine learning classification of SAR and optical images on Google Earth Engine, Int. J. Eng. Geosci. 8 (3) (2023) 239–250.

[2] H. Duysak, E. Yiğit, Investigation of the performance of different wavelet-based fusions of SAR and optical images using Sentinel-1 and Sentinel-2 datasets, Int. J. Eng. Geosci. 7 (1) (2022) 81–90.

[3] F. Perosanz, GNSS: a revolution for precise geopositioning, Comptes Rendus Phys. 20 (3) (2019) 171–175.

[4] A. Alonso-Díaz, M. Solla, J.L. Rodríguez, A. Elseicy, Integrated approach to improve Road Infrastructure Resilience through complementary Non-Destructive Techniques, ISPRS Ann. Photogramm. Remote Sens. Spat. Inf. Sci. 10 (4) (2024) 9–15.

[5] A. Alonso-Díaz, J. Casado-Rabasco, M. Solla, S. Lagüela, Using InSAR and GPR techniques to detect subsidence: application to the coastal area of "A Xunqueira" (NW Spain), Remote Sens. 15 (15) (2023) 3729.

[6] A. Alonso-Díaz, D. Roque, M. Solla, L.J. Nuno, Comparative analysis of MT-InSAR algorithms supported by GNSS data and corner reflectors: assessing performance and accuracy, Procedia Comput. Sci. 239 (2024) 1460–1466.

[7] Roque D. Displacement measurement through InSAR geodesy for structural health monitoring. 2020; Available from: https://repositorio.lnec.pt/handle/123456789/1016932.

[8] K. Xu, W. Gan, J. Wu, Z. Hou, A robust method for 3-D surface displacement fields combining GNSS and single-orbit InSAR measurements with directional constraint from elasticity model, GPS Solut. 26 (2) (2022) 1–16.

[9] Rodgers M, Deng F, Dixon TH, Glennie CL, James MR, Malservisi R, et al. Geodetic Applications to Geomorphology. In: Treatise on Geomorphology. Elsevier; 2022. p. 34–55.

[10] A. Ferretti, A. Fumagalli, E. Passera, A. Rucci, Insar data calibration in wide area processing, Int. Geosci. Remote Sens. Symp. (2022) 5101–5104.

[11] A. Allahvirdi-Zadeh, A. El-Mowafy, K. Wang, Precise orbit determination of cubesats using proposed observations weighting model, Int. Assoc. Geod. Symp. 154 (2023) 377–384.

[12] M. Manzoni, Fast and robust estimation of atmospheric phase screens using C-band spaceborne SAR and GNSS calibration, SpringerBriefs Appl. Sci. Technol. (2023) 131–140.

[13] B. Ju, X. Chang, D. Gu, X. Duan, J. Zhu, Z. Wang, Analysis and mitigation of the center-of-mass errors for InSAR baseline determination, Yaogan Xuebao/J. Remote Sens. 21 (4) (2017) 558–565.

[14] S. Zhao, D. Gu, B. Yi, D. Yi, Error analysis for the baseline estimation and calibration of distributed InSAR satellites, Int. Geosci. Remote Sens. Symp. 2016 (2016) 4179–4182.

[15] G. Farolfi, M. Del Soldato, S. Bianchini, N. Casagli, Exploitation of GNSS for calibrating space-borne SAR for the study of landsubsidence, Trends Earth Obs. 1 (2019) 118–121.

[16] B.K. Varugu, C.E. Jones, K. Wang, J. Chen, R.L. Osborne, G.Z. Voyiadjis, Optimized GNSS Cal/Val site selection for expanding InSAR viability in areas with low phase coherence: a case study for Southern Louisiana, IEEE J. Sel. Top. Appl. Earth Obs. Remote Sens. 17 (2024) 4875–4889.

[17] L. Bányai, I. Bozsó, E. Szűcs, K. Gribovszki, V. Wesztergom, Monitoring strategy of geological hazards using integrated three-dimensional InSAR and GNSS technologies with case study, Period. Polytech., Civ. Eng. 67 (4) (2023) 992–1000.

[18] G. Farolfi, A. Piombino, F. Catani, Fusion of GNSS and satellite radar interferometry: determination of 3D fine-scale map of present-day surface displacements in Italy as expressions of geodynamic processes, Remote Sens. 11 (4) (2019).

[19] M. Peng, M. Motagh, Z. Lu, Z. Xia, Z. Guo, C. Zhao, Q. Liu, Characterization and prediction of InSAR-derived ground motion with ICA-assisted LSTM model, Remote Sens. Environ. 301 (2024).

[20] M. Fabris, M. Battaglia, X. Chen, A. Menin, M. Monego, M. Floris, An integrated InSAR and GNSS approach to monitor land subsidence in the Po river delta (Italy), Remote Sens. 14 (21) (2022) 5578.

[21] V. Comerci, E. Vittori, The need for a standardized methodology for quantitative assessment of natural and anthropogenic land subsidence: the Agosta (Italy) gas field case, Remote Sens. 11 (10) (2019) 1178.

[22] H. Li, W. Wu, H. Guo, R.B. Langley, GPS and InSAR inversion for coseismic deformation field and slip distribution of the Ms7.0 Jiuzhaigou earthquake, ION 2019 Int. Tech. Meet. Proc. (2019) 676–685.

[23] F. Yang, J. Guo, X. Meng, J. Shi, L. Zhou, Establishment and assessment of a new GNSS precipitable water vapor interpolation scheme based on the GPT2w model, Remote Sens. 11 (9) (2019).

[24] N. Pierdicca, I. Maiello, F. Murgia, G. Venuti, E. Sansosti, S. Verde, et al., Atmospheric slant delay from SAR interferometry, GNSS and numerical weather prediction model: a comparison study in view of a geosynchronous SAR mission, Int. Geosci. Remote Sens. Symp. 2018 (2018) 4103–4106.

[25] M. Haley, M. Ahmed, E. Gebremichael, D. Murgulet, M. Starek, Land subsidence in the texas coastal bend: locations, rates, triggers, and consequences, Remote Sens. 14 (1) (2022) 192.

[26] G. Areggi, G. Pezzo, J.P. Merryman Boncori, L. Anderlini, G. Rossi, E. Serpelloni, D. Zuliani, L. Bonini, Present-day surface deformation in north-east Italy using InSAR and GNSS data, Remote Sens. 15 (6) (2023).

[27] M. Costantini, F. Minati, F. Trillo, A. Ferretti, E. Passera, A. Rucci, et al., EGMS: Europe-wide ground motion monitoring based on full resolution Insar processing of all Sentinel-1 acquisitions, Int. Geosci. Remote Sens. Symp. 2022 (2022) 5093–5096.

[28] I. Bozso, L. Banyai, A. Hooper, E. Szucs, V. Wesztergom, Integration of Sentinel-1 interferometry and GNSS networks for derivation of 3-D surface changes, IEEE Geosci. Remote Sens. Lett. 18 (4) (2021) 692–696.

[29] P. Dias, J. Catalao, F.O. Marques, Sentinel-1 InSAR data applied to surface deformation in Macaronesia (Canaries and Cape Verde), Procedia Comput. Sci. 138 (2018) 382–387.

[30] M. Komac, R. Holley, P. Mahapatra, H. van der Marel, M. Bavec, Coupling of GPS/GNSS and radar interferometric data for a 3D surface displacement monitoring of landslides, Landslides 12 (2) (2015) 241–257.

[31] K.G. Nikolakopoulos, A. Kyriou, I.K. Koukouvelas, N. Tomaras, E. Lyros, UAV, GNSS, and InSAR data analyses for landslide monitoring in a mountainous village in Western Greece, Remote Sens. 15 (11) (2023) 2870.

[32] D. Roque, J.N. Lima, D. Perissin, A.P. Falcão, J.V. Lemos, A.M. Fonseca, Integrated InSAR and GNSS monitoring subsystem for an arch dam and reservoir banks, J. Surv. Eng. 147 (3) (2021).

[33] A. Maltese, C. Pipitone, G. Dardanelli, F. Capodici, J.P. Muller, Toward a comprehensive dam monitoring: on-site and remote-retrieved forcing factors and resulting displacements (GNSS and PS–InSAR), Remote Sens. 13 (8) (2021) 1543, https://doi.org/10.3390/rs13081543.

[34] F. De Zan, A. Parizzi, F.R. Gonzalez, H. Ansari, G. Gomba, R. Brcic, M. Eineder, Insar error budget for large scale deformation, Int. Geosci. Remote Sens. Symp. 2019 (2019) 2042–2045.

[35] T. Gatsios, F. Cigna, D. Tapete, V. Sakkas, K. Pavlou, I. Parcharidis, Copernicus sentinel-1 MT-InSAR, GNSS and seismic monitoring of deformation patterns and trends at the methana volcano, Greece, Appl. Sci. 10 (18) (2020) 423.

[36] S. Yalvac, Validating InSAR-SBAS results by means of different GNSS analysis techniques in medium- and high-grade deformation areas, Environ. Monit. Assess. 192 (2) (2020) 120.

[37] F. Cigna, R.E. Ramírez, D. Tapete, Accuracy of sentinel-1 PSI and SBAS InSAR displacement velocities against GNSS and geodetic leveling monitoring data, Remote Sens. 13 (23) (2021) 4800.

[38] C. Danezis, D. Kakoullis, K. Fotiou, M. Pekri, M. Chatzinikos, C. Kotsakis, et al., CyCLOPS: a national integrated GNSS/InSAR strategic research infrastructure for monitoring geohazards and forming the next generation Datum of the Republic of Cyprus, Int. Assoc. Geod. Symp. 154 (2023) 289–302.

[39] Zhang X, Zong H, Yang H, Li Y, Shao Y, Hu L. Surface deformation monitoring in Dongchuan urban area between 2018-2020 based on PS-InSAR. 2022 3rd Int. Conf. Geol. Mapp Remote Sensing, ICGMRS 2022. 2022; 379–82.

[40] F. Cigna, A. Sowter, The relationship between intermittent coherence and precision of ISBAS InSAR ground motion velocities: ERS-1/2 case studies in the UK, Remote Sens. Environ. 202 (2017) 177–198.

[41] F. Orellana, D. Rivera, G. Montalva, J.L. Arumi, InSAR-Based early warning monitoring framework to assess aquifer deterioration, Remote Sens. 15 (7) (2023) 1786.

[42] G. Farolfi, S. Bianchini, N. Casagli, Integration of GNSS and satellite InSAR data: derivation of fine-scale vertical surface motion maps of Po Plain, Northern Apennines, and Southern Alps, Italy, IEEE Trans. Geosci. Remote Sens. 57 (1) (2019) 319–328.

[43] K. Fujiyama, S.M. Monitoring, MT. Shinnmoe's crater activity using the timeseries palsar-2 interferometry, Int. Geosci. Remote Sens. Symp. (2019) 1729–1732.

[44] LNEC - Laboratório Nacional de Engenharia Civil. (n.d.). História do LNEC. https://www.lnec.pt/pt/lnec/historia/, 2023 (accessed July 2023).

[45] O Campus do Laboratório Nacional de Engenharia Civil. https://www.lnec.pt/pt/lnec/campus/, 2023 (accessed 13 March 2023).

[46] A. Pepe, F. Calò, A review of interferometric synthetic aperture RADAR (InSAR) multi-track approaches for the retrieval of Earth's Surface displacements, Appl. Sci. 7 (12) (2017) 1264.

[47] V. Gagliardi, F. Tosti, L. Bianchini Ciampoli, M.L. Battagliere, L. D'Amato, A. M. Alani, A. Benedetto, Satellite remote sensing and non-destructive testing methods for transport infrastructure monitoring: advances, challenges and perspectives, Remote Sens. 15 (2) (2023) 418.

[48] D. Perissin, T. Wang, Repeat-pass SAR interferometry with partially coherent targets, IEEE Trans. Geosci. Remote Sens. 50 (1) (2012) 271–280.

[49] Software Manual – SARPROZ ©. Available from: https://www.sarproz.com/software-manual/ (accessed 14 June 2023).

[50] S. Jin, Q. Wang, G. Dardanelli, A review on multi-GNSS for earth observation and emerging applications, Remote Sens. 14 (16) (2022) 3930.

[51] Goad CC, Goodman L. A modified Hopfield tropospheric refraction correction model. In: Fall Annual Meeting American Geophysical Union; 1974; San Francisco, California.

[52] Precise Point Positioning. Available from: https://webapp.csrs-scrs.nrcan-rncan.gc.ca/geod/tools-outils/ppp.php/ (accessed 22 July 2023).

[53] F. Dentz, L. van Halderen, P. Boudewijn, S.S. Esfahany, C. Slobbe, T. Wortel, "POSEIDON" on the Potential of Satellite Radar Interferometry for Monitoring Dikes of the Netherlands—A Technical Feasibility Study, Delft University of Technology, 2006.